Article

Increased hyaluronan by naked mole-rat Has2 improves healthspan in mice

https://doi.org/10.1038/s41586-023-06463-0

Received: 30 October 2022

Accepted: 20 July 2023

Published online: 23 August 2023

Check for updates

Zhihui Zhang[1], Xiao Tian[1], J. Yuyang Lu[1], Kathryn Boit[1], Julia Ablaeva[1], Frances Tolibzoda Zakusilo[1], Stephan Emmrich[1], Denis Firsanov[1], Elena Rydkina[1], Seyed Ali Biashad[1], Quan Lu[1], Alexander Tyshkovskiy[2,3], Vadim N. Gladyshev[2], Steve Horvath[4,5], Andrei Seluanov[1,6] ✉ & Vera Gorbunova[1,6] ✉

Abundant high-molecular-mass hyaluronic acid (HMM-HA) contributes to cancer resistance and possibly to the longevity of the longest-lived rodent—the naked mole-rat[1,2]. To study whether the benefits of HMM-HA could be transferred to other animal species, we generated a transgenic mouse overexpressing naked mole-rat hyaluronic acid synthase 2 gene (nmr*Has2*). nmr*Has2* mice showed an increase in hyaluronan levels in several tissues, and a lower incidence of spontaneous and induced cancer, extended lifespan and improved healthspan. The transcriptome signature of nmr*Has2* mice shifted towards that of longer-lived species. The most notable change observed in nmr*Has2* mice was attenuated inflammation across multiple tissues. HMM-HA reduced inflammation through several pathways, including a direct immunoregulatory effect on immune cells, protection from oxidative stress and improved gut barrier function during ageing. These beneficial effects were conferred by HMM-HA and were not specific to the nmr*Has2* gene. These findings demonstrate that the longevity mechanism that evolved in the naked mole-rat can be exported to other species, and open new paths for using HMM-HA to improve lifespan and healthspan.

Naked mole-rats are mouse-size rodents that display exceptional longevity, with a maximum lifespan of over 40 years[3]. Naked mole-rats are protected from multiple age-related diseases[4,5]. Previously, we have identified an anti-cancer mechanism in the naked mole-rat named early contact inhibition[1] that is mediated by abundant HMM-HA[2]. Naked mole-rat tissues are highly enriched for HMM-HA compared with mouse and human tissues.

Hyaluronan is a non-protein component of the extracellular matrix consisting of repeating disaccharide chains of *N*-acetyl-glucosamine and glucuronic acid that affects biomechanical properties of tissues and interacts with cell receptors[6,7]. The length of hyaluronan can range from an oligomer to an extremely long-form up to millions of Daltons, and the biological functions of hyaluronan depend on its molecular mass. Low-molecular-mass HA (LMM-HA) is associated with inflammation, tissue injury and cancer metastasis[8–11], whereas HMM-HA improves tissue homeostasis[12] and shows anti-inflammatory[13,14] and antioxidant properties[15]. The HMM-HA (>6.1 MDa) produced by naked mole-rats has unique cytoprotective properties[16]. The hyaluronan content is determined by the balance of hyaluronan synthesis and degradation[17]. Has2 mainly produces HMM-HA and shows higher expression in naked mole-rats compared with in mice and humans[2]. Naked mole-rat tissues also show lower activity of hyaluronidases, resulting in the massive accumulation of HMM-HA[2]. Age-related sterile inflammation has emerged as an important driving force of ageing and age-related diseases[18,19]. Thus, the anti-inflammatory functions of HMM-HA may confer anti-ageing effects. To test whether anti-cancer and potential anti-ageing effects of HMM-HA can be recapitulated in species other than the naked mole-rat, we generated and characterized a mouse model overexpressing naked mole-rat *Has2* gene (nmr*Has2* mice).

Generation of nmr*Has2* mice

As naked mole-rats accumulate HMM-HA in the majority of their tissues, to recreate this phenotype in mice, we chose to express the naked mole-rat *Has2* gene (nmr*Has2*) in mice using a ubiquitous CAG promoter. In the naked mole-rat, HMM-HA begins to accumulate postnatally[1] as it is not compatible with rapid cell proliferation required during embryogenesis. We therefore controlled nmr*Has2* expression temporally using a Lox-STOP cassette. Expression of the nmr*Has2* gene was induced by injections of tamoxifen at 3 months of age (Fig. 1a). Both nmr*Has2* and control mice received tamoxifen injections.

Overexpression of nmr*Has2* mRNA was detected in multiple tissues of nmr*Has2* mice (Extended Data Table 1). HABP staining showed a stronger hyaluronan signal in the muscle, kidneys and intestines of both male and female nmr*Has2* mice compared with the controls (Fig. 1b–d and Extended Data Fig. 1a–c). Furthermore, analysis using pulse-field

[1]Department of Biology, University of Rochester, Rochester, NY, USA. [2]Division of Genetics, Department of Medicine, Brigham and Women's Hospital and Harvard Medical School, Boston, MA, USA. [3]Belozersky Institute of Physico-Chemical Biology, Moscow State University, Moscow, Russia. [4]Department of Biostatistics, Fielding School of Public Health, University of California Los Angeles, Los Angeles, CA, USA. [5]Department of Human Genetics, David Geffen School of Medicine, University of California Los Angeles, Los Angeles, CA, USA. [6]Department of Medicine, University of Rochester Medical Center, Rochester, NY, USA. ✉e-mail: andrei.seluanov@rochester.edu; vera.gorbunova@rochester.edu

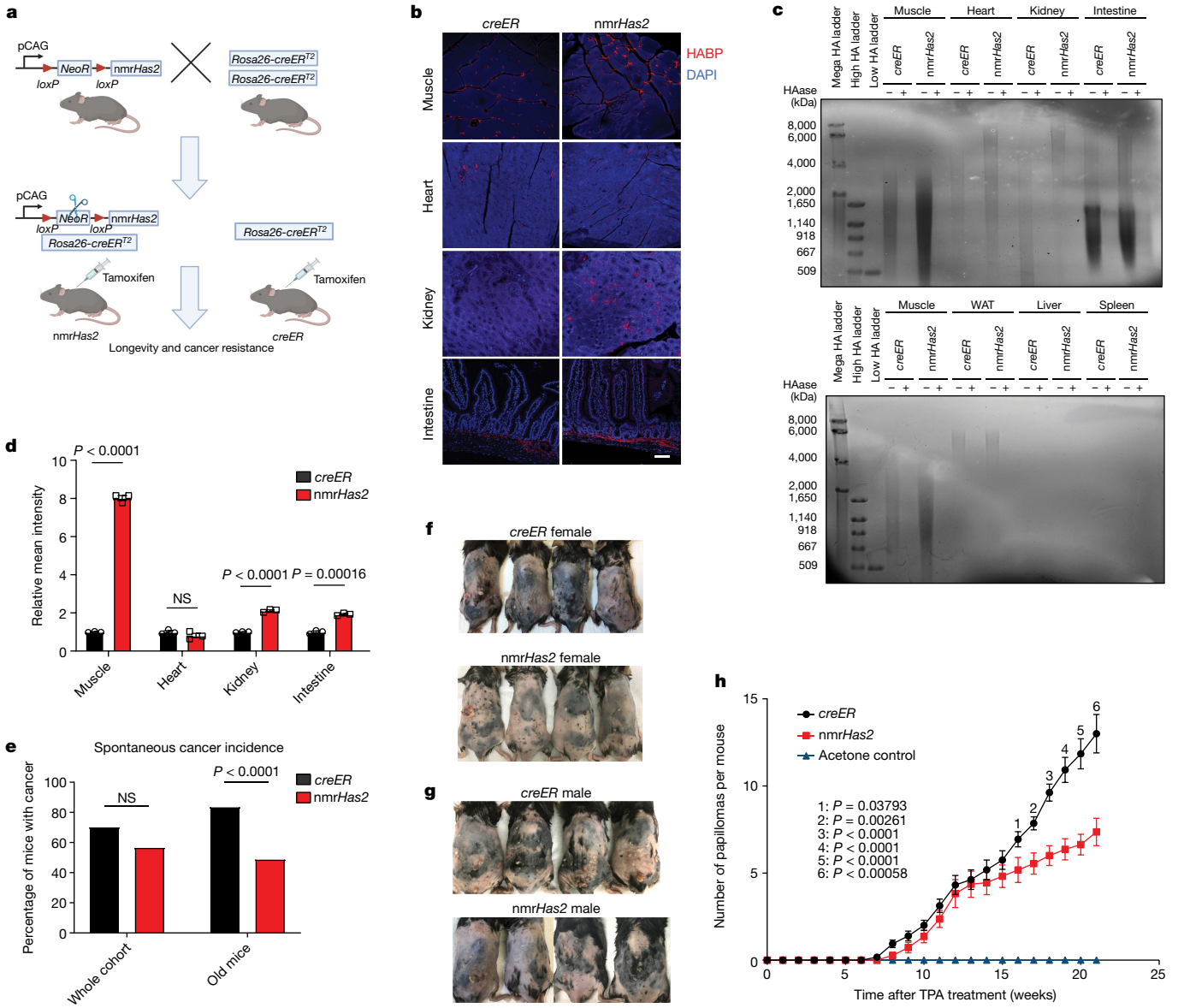

Fig. 1 | Transgenic mice overexpressing nmr*Has2* are resistant to both spontaneous and induced cancer. a, The breeding strategy for nmr*Has2* mice. Mice heterozygous for the nmr*Has2* transgene were bred with mice homozygous for *Rosa26-creER*^{T2} to obtain double-heterozygous nmr*Has2*;*creER* progeny. Single-heterozygous *creER* progeny were used as controls. Tamoxifen was injected at 2–3 months of age to induce nmr*Has2* expression. *creER* mice also received tamoxifen. **b**, Representative pictures of HABP staining in multiple organs of female mice. Scale bar, 50 µm. **c**, Pulse-field gel showing that nmr*Has2* mice have higher molecular mass and more abundant HA in multiple tissues (female mice are shown). HA was extracted from 200 mg of pooled tissue from two individuals. HAase-treated samples were run in parallel to confirm the specificity of HA staining. HA from the muscle was loaded onto both gels as a cross reference. WAT, white adipose tissue. **d**, Quantification of relative HABP fluorescence intensity shown in **b**. $n = 3$ biological replicates (squares). **e**, Old nmr*Has2* mice ($n = 74$) have a much lower spontaneous cancer incidence compared with *creER* mice ($n = 81$). Pooled female and male mice. Old mice were older than 27 months. Statistical analysis was performed using a two-tailed χ^2 test. **f**, Representative pictures of female mice after 20 weeks of DMBA/TPA treatment. **g**, Representative pictures of male mice after 20 weeks of DMBA/TPA treatment. **h**, nmr*Has2* mice are more resistant to DMBA/TPA-induced skin papilloma. Pooled female and male mice. $n = 7$ (acetone treated), $n = 13$ (*creER*) and $n = 11$ (nmr*Has2*) mice. *P* values were calculated using two-tailed unpaired *t*-tests and are indicated in the graphs. NS, not significant. For **d**, **e** and **h**, data are mean ± s.e.m. (**d** and **h**) or mean (**e**).

gel electrophoresis showed that hyaluronan extracted from the tissues of nmr*Has2* mice was more abundant and had a higher molecular mass in the muscle, heart, kidneys and small intestine (Fig. 1c and Extended Data Fig. 1b). Hyaluronan levels in the liver and spleen were very low, which is consistent with these tissues being the sites of hyaluronan breakdown[20]. Notably, despite the high nmr*Has2* mRNA levels in most mouse organs, we observed only a mild increase in hyaluronan, probably due to high hyaluronidase activity in mouse tissues compared with the naked mole-rat[2].

nmr*Has2* mice are resistant to both spontaneous and induced cancer

To examine the effect of HMM-HA on lifespan and spontaneous cancer incidence, we set up ageing cohorts of 80–90 mice of both genotypes. The majority of mice died from cancer, which is consistent with earlier reports that lymphomas are the common end point for aged C57BL/6 mice[21]. nmr*Has2* mice showed lower spontaneous cancer incidence, with 57% of nmr*Has2* mice dying from cancer compared with 70% of

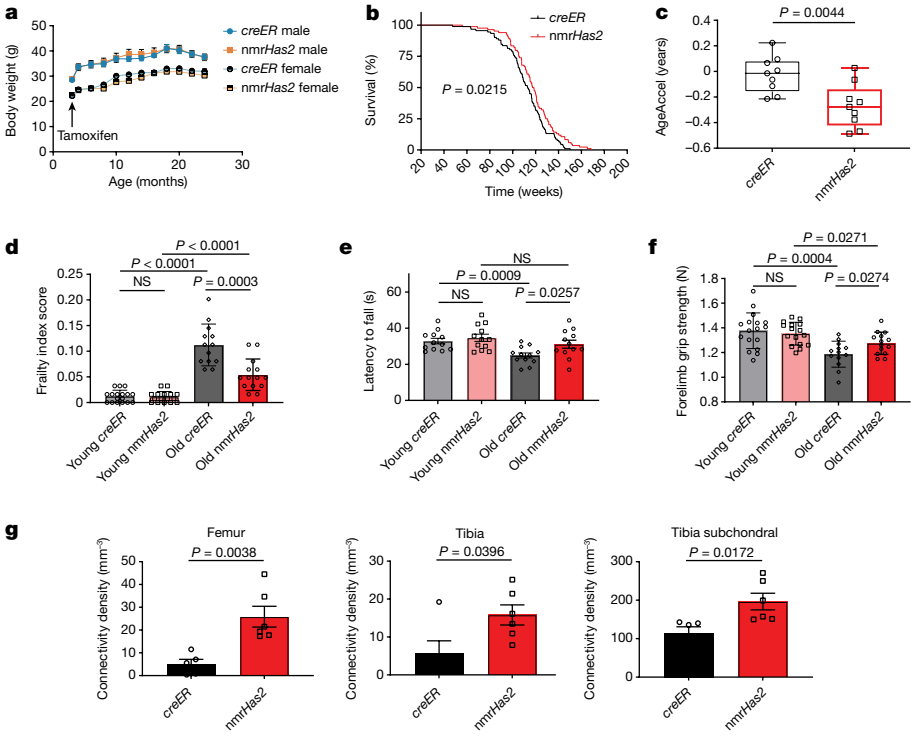

Fig. 2 | nmr*Has2* mice have an extended lifespan and improved healthspan. **a**, Overexpression of nmr*Has2* did not affect the body weight of the mice. The body weight of mice was measured before tamoxifen injection, then once every month until the mice reached 24 months of age. $n = 10$ (*creER* male and female), $n = 9$ (nmr*Has2* female) and $n = 11$ (nmr*Has2* male) mice. **b**, nmr*Has2* mice ($n = 84$) have an extended median and maximum lifespan compared with *creER* mice ($n = 91$). Pooled female and male mice. The *P* value was calculated using a two-tailed log-rank test. **c**, Old nmr*Has2* mice display a younger biological age. Liver DNA from 24-month-old nmr*Has2* ($n = 9$) and age-matched *creER* ($n = 9$) mice was used for the methylation clock assay. The methylation age of each mouse was normalized to its chronological age to calculate AgeAccel. The box plot shows the median (centre line), the first to third quartiles (box limits), and the minimum and maximum values (whiskers). *P* values were calculated using two-tailed unpaired *t*-tests. **d**, Frailty index scores of *creER* and nmr*Has2* mice at 5 and 24 months of age. Pooled female and male mice. $n = 17$ (young *creER*), $n = 16$ (young nmr*Has2*), $n = 13$ (old *creER*) and $n = 14$ (old nmr*Has2*) mice. **e**, Rotarod performance of *creER* and nmr*Has2* mice at 5 and 24 months of age. Six female mice and six male mice were used for each group. **f**, The forelimb grip strength performance of *creER* and nmr*Has2* mice at 5 and 24 months of age. Pooled female and male mice. $n = 17$ (young *creER*), $n = 16$ (young nmr*Has2*), $n = 13$ (old *creER*) and $n = 14$ (old nmr*Has2*) mice. **g**, Old female nmr*Has2* mice have a higher bone connectivity density. Hindlimb bones from 24-month-old animals were taken for micro-CT scan. $n = 5$ (*creER*) and $n = 6$ (nmr*Has2*) mice. *P* values were calculated using two-tailed unpaired *t*-tests; *P* values are indicated in the graphs. For **a** and **c**–**g**, data are mean ± s.e.m. The symbols in **c**–**g** represent biological replicates. Adjustments were made for multiple comparisons.

the mice in the control *creER* group (Fig. 1e). This difference was further amplified for the oldest age group. For mice older than 27 months, cancer incidence was 83% for *creER* mice and 49% for nmr*Has2* mice (Fig. 1e). This phenotype was the same across both sexes (Extended Data Fig. 1d,e).

nmr*Has2* mice showed accumulation of HA in the skin (Extended Data Fig. 1f). To test the resistance of nmr*Has2* mice to chemically induced skin tumorigenesis, we treated young mice with DMBA/TPA. Sixteen weeks after TPA treatment, nmr*Has2* mice formed significantly fewer papillomas compared with the age-matched controls among female mice, male mice and the two sexes combined (Fig. 1f–h and Extended Data Fig. 1g,h). These results indicate that production of HMM-HA protected mice from both spontaneous and induced cancer.

nmr*Has2* mice have increased lifespan

Mice of both genotypes had a similar body weight throughout their life (Fig. 2a). nmr*Has2* mice showed an increase of 4.4% in median lifespan and 12.2% in maximum lifespan (Fig. 2b). The lifespan increase was different for each sex. Whereas female mice showed a more prominent 9% increase in their median lifespan (Extended Data Fig. 2a), male mice showed a more prominent 16% increase in their maximum lifespan (Extended Data Fig. 2b). Furthermore, nmr*Has2* mice exhibited a younger biological age, as determined by measuring the epigenetic age in livers of 24 months old mice using HorvathMammalMethylChip40 (refs. 22,23). Epigenetic age was compared with chronological age to quantify age acceleration. The methylation age of *creER* mice was close to their chronological age, whereas nmr*Has2* mice showed approximately −0.2 years of age acceleration in both sexes (Fig. 2c and Extended Data Fig. 2c–e). This result indicates that old nmr*Has2* mice have a significantly younger biological age than their chronological age. We also examined methylation levels of the 6,553 CpG sites that were previously shown to undergo methylation changes during ageing[24]. Our analysis revealed that, of the 6,553 CpG sites, 165 were differentially methylated between nmr*Has2* mice and *creER* mice. Among these sites, 145 sites that gain methylation during ageing showed lower methylation in nmr*Has2* mice compared with in the age-matched controls; and 20 CpG sites that lose methylation during ageing showed higher methylation in nmr*Has2* mice compared with in the age-matched controls (Extended Data Fig. 2f,g and Supplementary Table 2).

nmr*Has2* mice have an improved healthspan

To provide a quantitative measure of health, we used a mouse frailty index[25], which combined 31 parameters, including body weight, temperature, coat condition, grip strength, mobility, vision and

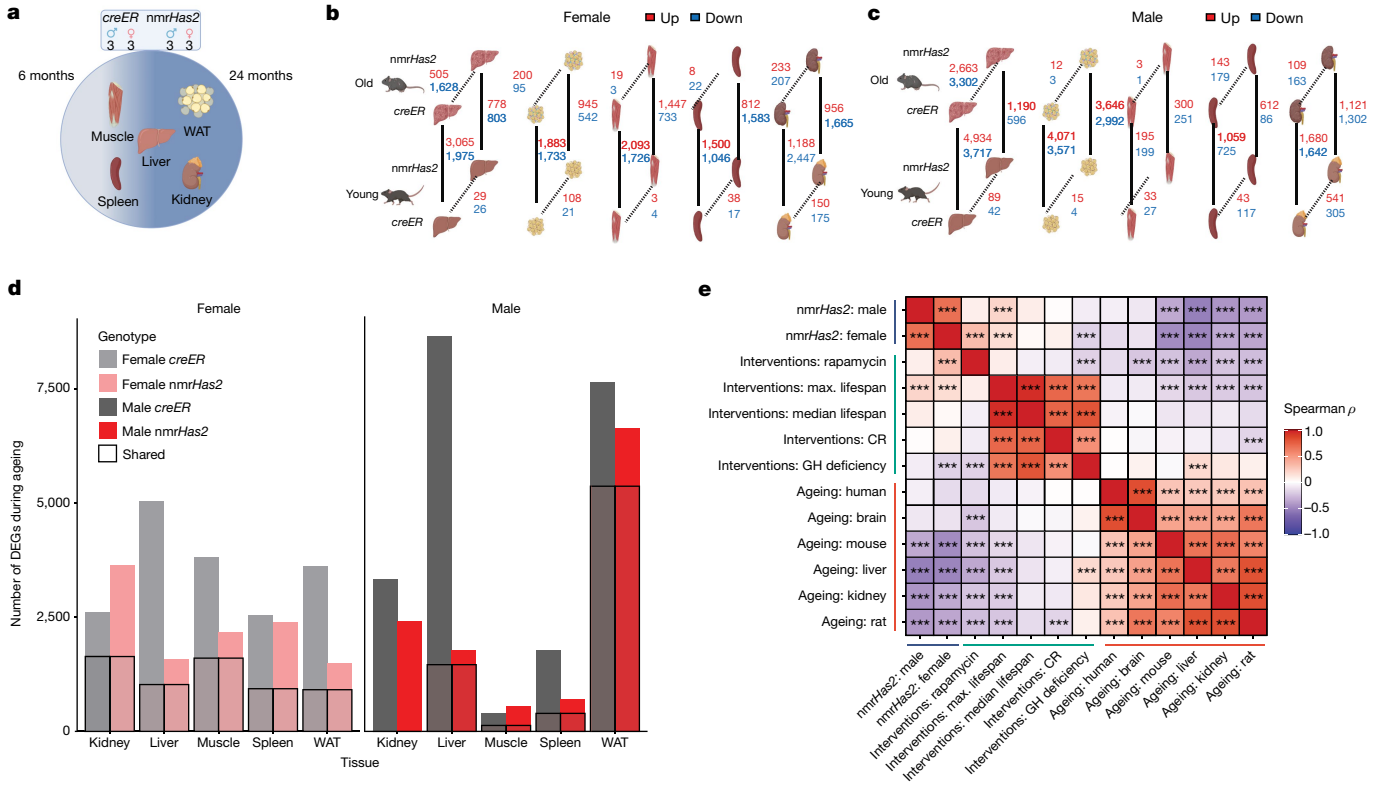

Fig. 3 | The transcriptome of nmr*Has2* mice undergoes fewer changes during ageing compared with the transcriptome of *creER* controls. a, The sequencing and sampling strategy. The liver, muscle, white adipose tissue, kidneys and spleen of 6- and 24-month-old *creER* and nmr*Has2* mice were analysed using RNA-seq. Three biological replicates for each sex, age group and genotype were used. **b**, Gene expression changes in female mice. Two parameters were compared: genotype (dashed lines) and age (solid lines). **c**, Gene expression changes in male mice. Two parameters were compared: genotype (dashed lines) and age (solid lines). **d**, The effects of ageing on the transcriptome. The number of genes of which the expression changed with age in either direction; the boxed areas represent genes that underwent changes in both genotypes. **e**, The association between nmr*Has2* effect on liver gene expression in old mice and signatures of lifespan-extending interventions and mammalian ageing. Signatures of ageing, lifespan-extending interventions and nmr*Has2* are shown in red, green and blue, respectively. CR, caloric restriction; GH, growth hormone. Adjusted *P* values are shown in Supplementary Table 3.

hearing. The frailty index score increased with age for both nmr*Has2* and *creER* mice. However, the frailty index score of old nmr*Has2* mice was substantially lower than that of the age-matched control group (Fig. 2d).

Rotarod performance[26] was assessed to measure the locomotion and coordination of mice. The latency-to-fall time became significantly shorter for old *creER* mice compared with the young *creER* mice. However, old nmr*Has2* mice maintained youthful performance (Fig. 2e). The grip strength of both *creER* and nmr*Has2* mice decreased with age but old nmr*Has2* mice maintained a better performance compared with the old *creER* mice (Fig. 2f).

Osteoporosis is an important component of healthspan in female mice[27], with connectivity density decreasing during ageing[28]. Old nmr*Has2* female, but not male, mice showed higher connectivity density in the femur, tibia and tibia subchondral region compared with the age-matched control mice (Fig. 2g and Extended Data Fig. 2h). Cumulatively, our results show that increased levels of HMM-HA in mice improves multiple parameters of healthspan.

Gene expression analysis points to reduced inflammation in nmr*Has2* mice

For most organs, nmr*Has2* mice showed fewer transcriptome changes during ageing compared with the *creER* controls, in both female and male mice, which means that the transcriptome of nmr*Has2* mice is less perturbed during ageing (Fig. 3a–d). We next examined whether the transcriptome of nmr*Has2* mice shares any common features with transcriptomic changes induced by other pro-longevity interventions such as rapamycin, calorie restriction and growth-hormone receptor knockout. We performed a hierarchical clustering analysis using RNA-sequencing (RNA-seq) data from livers of young and old nmr*Has2* mice with expression data published for other interventions[29]. We built a heat map based on Pearson correlation coefficients across all datasets (Extended Data Fig. 3a). Notably, the transcriptomes of neither young nor old nmr*Has2* mice showed a clear correlation with any transcriptome data derived from the livers of mice subjected to other pro-longevity interventions. This result may suggest that increased levels of HMM-HA generated a new pro-longevity transcriptomic signature (Extended Data Fig. 3a). To test whether the observed outcome is not due to noise generated by using the entire transcriptome data, we calculated the Spearman correlation between the top 400 gene expression changes induced by nmrHas2 expression in old mice and those associated with ageing and established lifespan-extending interventions[30]. We observed significant positive correlations between the transcriptomic profiles of nmr*Has2* mice and the signatures of rapamycin and mouse maximum lifespan affected by longevity interventions (Fig. 3e). On the other hand, the effect of nmr*Has2* expression was negatively associated with multiple signatures of ageing and biomarkers of interventions associated with growth hormone deficiency. The observed correlations were further amplified at the level of enriched pathways, estimated using gene set enrichment analysis (GSEA). Thus, at the functional level, nmr*Has2* signatures were positively associated with patterns of maximum and median lifespan, caloric restriction and rapamycin, and negatively correlated with all ageing signatures

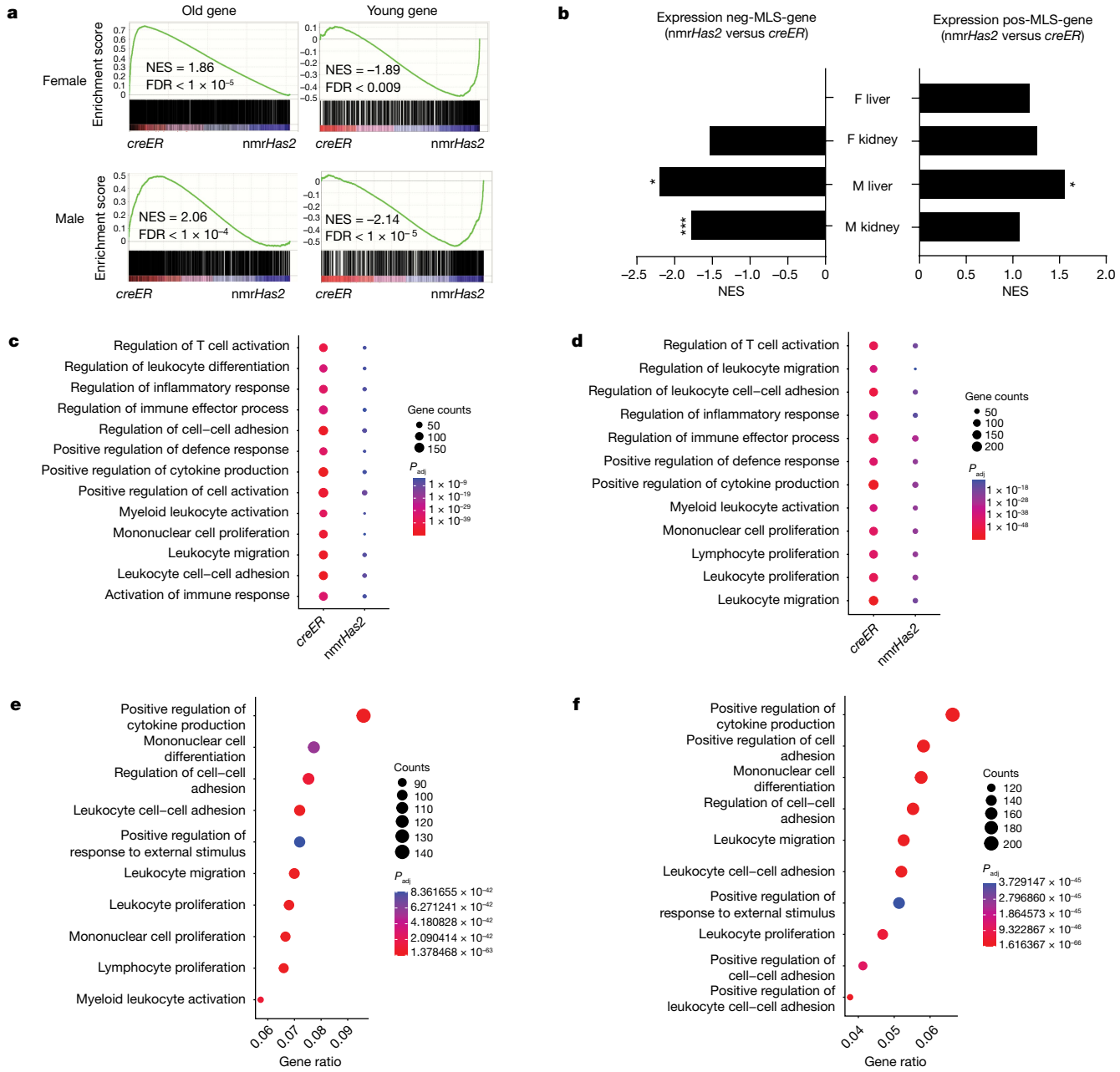

Fig. 4 | nmr*Has2* mice display a younger transcriptome signature and reduced inflammation during ageing. a, GSEA plots showing that the young gene set is upregulated, and the old gene set is downregulated in the liver of old nmr*Has2* mice of both sexes. NES, normalized enrichment score. **b**, GSEA shows that the pos-MLS gene set was upregulated in the liver and kidneys of nmr*Has2* mice. The neg-MLS gene set was downregulated in the liver and kidneys of old nmr*Has2* mice. *False-discovery rate (FDR)-adjusted $P < 0.05$, ***FDR-adjusted $P < 1 \times 10^{-5}$. **c**,**d**, GO term enrichment analysis shows that the livers of old female (**c**) and male (**d**) nmr*Has2* mice have fewer inflammation-related pathways upregulated during ageing. **e**,**f**, GO term enrichment analysis shows that inflammation-related pathways are downregulated in the livers of old female (**e**) and male (**f**) nmr*Has2* mice.

(Extended Data Fig. 3b). The pro-longevity and anti-ageing effects of nmr*Has2* expression were driven by significant downregulation of pathways associated with interleukin and interferon signalling, and by upregulation of genes involved in oxidative phosphorylation, respiratory electron transport and mitochondrial translation (Extended Data Fig. 3c,d). Notably, nmr*Has2* mice demonstrated stronger downregulation of inflammation and senescence compared with other examined lifespan-extending interventions. Taken together, our results suggest that nmr*Has2* expression in mice generates both pro-longevity and anti-ageing transcriptomic changes, some of which are shared with other established interventions while others appear to be unique characteristics of nmr*Has2* model.

By reanalysing the published transcriptome data from mice of different ages[31], we determined the signature of gene expression changes during ageing. The genes upregulated in old mice were defined as the 'old' gene set and the genes upregulated in young mice were defined as the 'young' gene set. Compared with old *creER* mice that showed upregulation of old gene sets in the liver, old nmr*Has2* mice liver showed upregulation of the young gene set (Fig. 4a). Although some tissues did not exhibit statistical significance, the trend displays high consistency across all of the tissues that we sequenced (Extended Data Fig. 4a–e). This result indicates that tissues of old nmr*Has2* mice were shifted towards the young state in both sexes at the transcriptomic level.

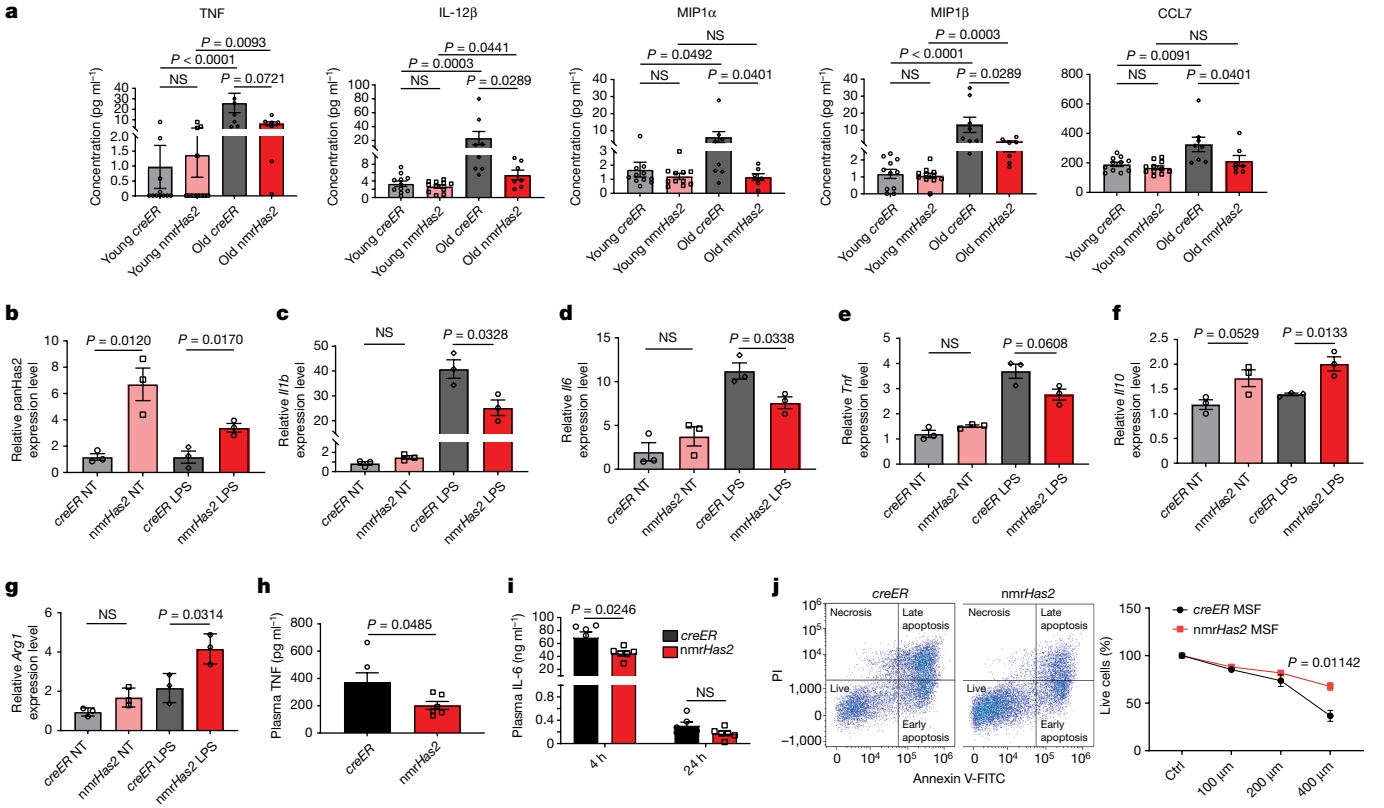

Fig. 5 | nmrHas2 reduces the pro-inflammatory response in vitro and in vivo and protects cells from oxidative stress. a, Luminex multiplex immunoassay shows that old female nmr*Has2* mice have reduced levels of multiple inflammatory cytokines and chemokines. $n = 11$ (young *creER* and nmr*Has2*), $n = 8$ (old *creER*) and $n = 7$ (old nmr*Has2*) mice. **b**, BMDMs from nmr*Has2* mice have significantly upregulated Has2 levels. NT, not treated with LPS. **c**–**e**, BMDMs from nmr*Has2* mice have lower levels of pro-inflammatory *Il1b* (**c**), *Il6* (**d**) and *Tnf* (**e**) mRNA after LPS challenge. **f**,**g**, BMDMs from nmr*Has2* mice have higher levels of anti-inflammatory *Il10* (**f**) and *Arg1* (**g**) mRNA after LPS challenge. **h**,**i**, nmr*Has2* mice have significantly lower plasma TNF (**h**) and IL-6 (**i**) levels 4 h after LPS challenge. $n = 3$ 5-month-old male mice. **j**, Skin fibroblasts isolated from nmr*Has2* mice are more resistant to H_2O_2 treatment. Skin fibroblasts were isolated from 5-month-old male mice. $n = 3$. MSF, mouse skin fibroblast. For **b**–**g**, BMDMs were isolated from 5-month-old male mice ($n = 3$). *P* values were calculated using two-tailed unpaired Mann–Whitney *U*-tests (**a**) and two-tailed unpaired *t*-tests (**b**–**j**); *P* values are indicated in the graphs. For **a**–**j**, data are mean ± s.e.m. The symbols in **a**–**i** represent biological replicates.

In our previous comparative cross-species study, by analysing the transcriptomes of 26 species, we obtained gene sets of which the expression positively or negatively correlates with maximum lifespan, named the pos-MLS gene set and neg-MLS gene set, respectively[32]. By using those gene sets for the GSEA, we found that the pos-MLS gene set is upregulated in the livers and kidneys of old nmr*Has2* mice of both sexes. By contrast, the neg-MLS gene set was downregulated in the liver and kidneys of old male nmr*Has2* mice and in the kidneys of old female nmr*Has2* mice (Fig. 4b). This result suggests that the nmr*Has2* transgene facilitates the expression of pro-longevity genes (genes that are highly expressed in long-lived species) and represses the expression of genes that are more highly expressed in short-lived species.

By comparing genes of which the expression changed with ageing within each genotype, we found that *creER* mice have more upregulated genes involved in the inflammatory response in the liver and spleen of both sexes, in the kidneys of male mice and in the white adipose tissue and muscle of female mice (Fig. 4c,d and Extended Data Fig. 5a–h). This result indicates that HMM-HA attenuates age-related inflammation in multiple tissues.

Moreover, we analysed the differentially expressed genes (DEGs) between two genotypes of mice at the same age. Expression of nmr*Has2* had very mild effects on the overall transcriptome of young mice, and there were very few DEGs observed between young nmr*Has2* and *creER* mice (Fig. 3b,c). For old mouse organs, we picked the liver that showed most DEGs between nmr*Has2* and *creER* mice for the Gene Ontology (GO) term enrichment analysis. Our results revealed that both female and male nmr*Has2* liver showed reduced expression of inflammatory-related genes and higher expression of genes involved in normal liver functions such as nutrient metabolism. This result indicates that the liver of old nmr*Has2* mice showed reduced inflammation and better-preserved functions compared with the controls (Fig. 4e,f and Extended Data Fig. 5i,j). Overall, these results demonstrate that nmr*Has2* mice display reduced age-related inflammation.

HA reduces inflammation and oxidative stress

An analysis of 36 cytokines and chemokines in mouse plasma showed upregulation of several targets in male mice, but the trend did not reach statistical significance due to high individual variability (Extended Data Fig. 6). In female mice, almost all cytokine and chemokine levels were increased during ageing, which is consistent with the effect of sex hormones on immunity during ageing[33]. Notably, the majority of pro-inflammatory cytokines and chemokines were lower in old nmr*Has2* mice compared with in the age-matched controls (Extended Data Fig. 7). The differences for the pro-inflammatory cytokines IL-12p40, MIP1α and MIP1β, and the chemokine CCL7 reached statistical significance (Fig. 5a). Collectively, the transcriptome and cytokine data show that overexpression of nmr*Has2* attenuates inflammaging in mice.

HMM-HA molecules exert anti-inflammatory and immunoregulatory effects[34]. It was reported that HMM-HA represses classic pro-inflammatory M1 macrophage activation but promotes an anti-inflammatory alternative M2 macrophage activation[35]. We isolated

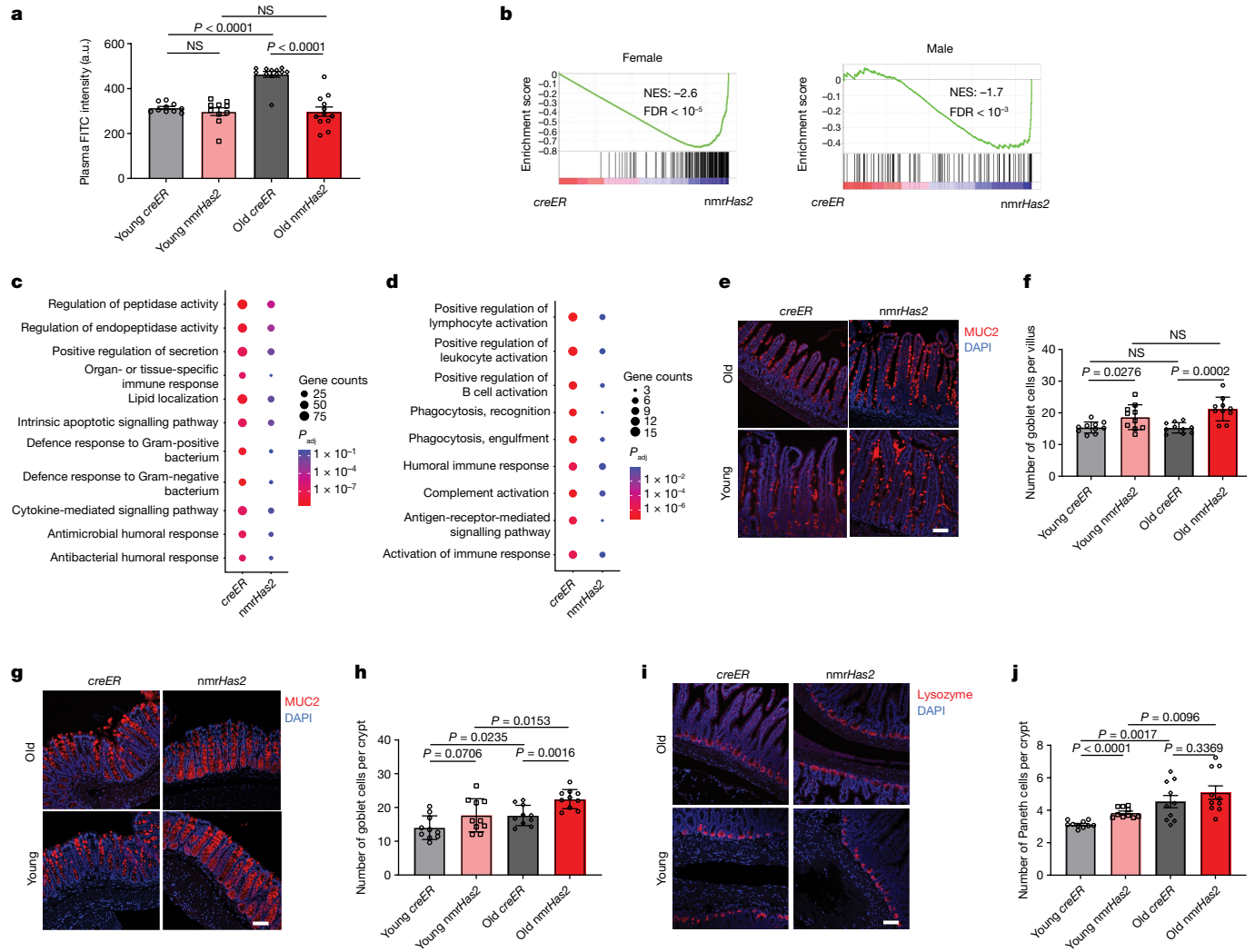

Fig. 6 | nmr*Has2* mice are protected from age-related loss of gut barrier function. a, nmr*Has2* mice have a less leaky gut compared with the age-matched controls. Pooled female and male mice. $n = 10$ (young *creER* and nmr*Has2*) and $n = 12$ (old *creER* and old nmr*Has2*) mice. a.u., arbitrary units. **b**, GSEA showing that old nmr*Has2* mice have a younger intestine at the transcriptome level for both sexes. **c**,**d**, GO term analysis showing that the small intestine of old nmr*Has2* mice has fewer inflammatory-related pathways upregulated during ageing for both female (**c**) and male (**d**) mice. **e**, Representative pictures of goblet cell staining in the small intestine of nmr*Has2* and *creER* mice. Scale bar, 50 µm. **f**, Quantification of goblet cells in the small intestine of 7- and 24-month-old mice (shown in **e**). Pooled female and male mice ($n = 10$). **g**, Representative pictures of goblet cell staining in the distal colon of nmr*Has2* and *creER* mice. Scale bar, 50 µm. **h**, Goblet cell counts in the distal colon of 7- and 24-month-old mice (shown in **g**). Pooled female and male mice ($n = 10$). **i**, Representative pictures of Paneth cell staining in the small intestine of nmr*Has2* and *creER* mice. Scale bar, 50 µm. **j**, Paneth cell counts in the small intestine of 7- and 24-month-old mice. Pooled female and male mice ($n = 10$). For **a**, **f**, **h** and **j**, *P* values were calculated using two-tailed unpaired *t*-tests; *P* values are indicated in the graphs. For **a**, **f**, **h** and **j**, data are mean ± s.e.m. The symbols represent biological replicates. Adjustments were made for multiple comparisons.

bone-marrow-derived macrophages (BMDMs) from young *creER* and nmr*Has2* mice and cultured them in vitro. Macrophages from male nmr*Has2* mice showed a sixfold increase in pan*Has2* mRNA expression compared with macrophages from male *creER* mice (Fig. 5b). To check the activation of macrophages, we treated BMDMs with *Escherichia coli* lipopolysaccharide (LPS). The level of Has2 decreased after LPS treatment but remained significantly higher for nmr*Has2* macrophages isolated from male mice. The level of two major HAases, HYAL1 and HYAL2, also decreased after LPS treatment (Extended Data Fig. 8c–f). nmr*Has2* macrophages from male mice produced significantly lower levels of pro-inflammatory *Il1b* and *Il6* (Fig. 5c,d) compared with the *creER* macrophages. *Tnf* also showed lower levels in nmr*Has2* cells but the effect did not reach statistical significance (Fig. 5e). Notably, male nmr*Has2* macrophages produced higher levels of anti-inflammatory *Il10* and *Arg1* (encoding arginase 1) after LPS challenge (Fig. 5f,g).

To test whether the anti-inflammatory effect is due to increased HMM-HA rather than to an unknown function of nmrHas2, we generated Raw264.7 macrophage cell lines overexpressing either mouse *Has2* or nmr*Has2* under the control of the same CAG promoter and challenged them with LPS. Macrophages overexpressing any form of HAS2 exhibited an anti-inflammatory effect similar to that seen in primary macrophages, implying that the anti-inflammatory effect arose from the production of HMM-HA (Extended Data Fig. 8b).

Macrophages from female nmr*Has2* mice had a lower HAS2 level compared with macrophages from nmr*Has2* male mice. After treatment with LPS, nmrHas2 levels in female nmr*Has2* macrophages dropped to the same level as that in female *creER* macrophages (Extended Data Fig. 8a). As a consequence, female mice did not show expression differences in cytokines after LPS challenge (data not shown). LPS stimulation triggered similar HAS2 and hyaluronidase (HAase) changes in

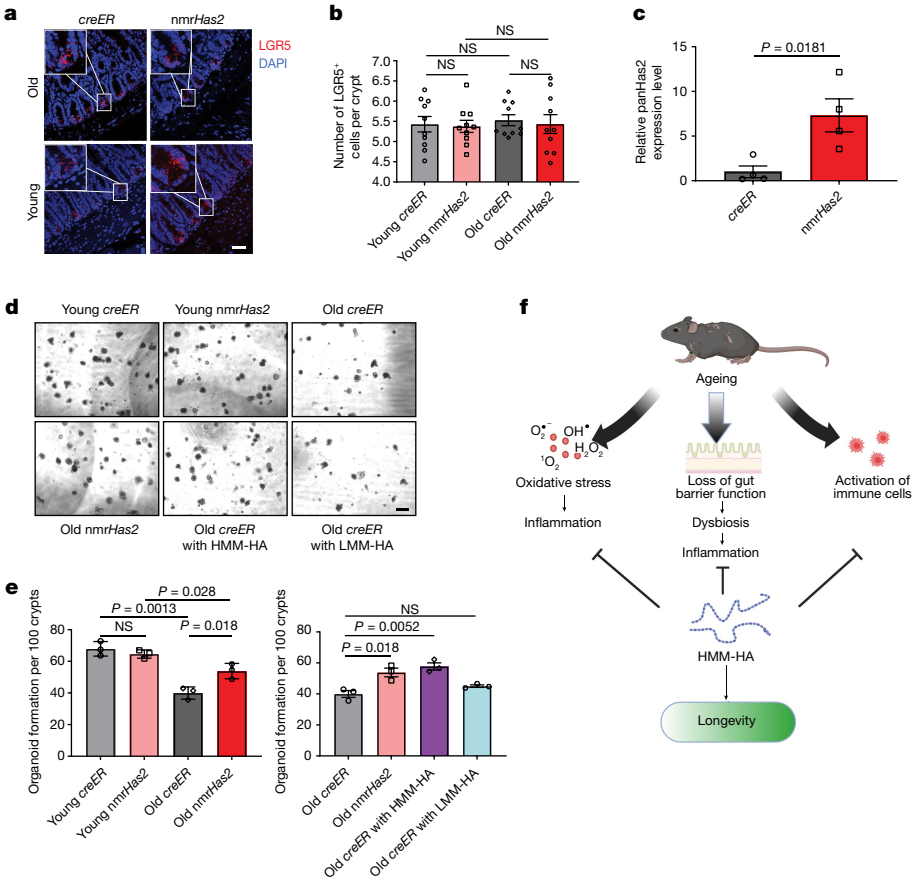

Fig. 7 | HMM-HA improves the maintenance of ISCs during ageing. **a**, Representative pictures of LGR5 in situ hybridization in the small intestine of young and old nmr*Has2* and *creER* mice. Scale bar, 50 µm. **b**, LGR5$^+$ ISC counts in the small intestines of 7- and 24-month-old mice. Pooled female and male mice ($n = 10$). **c**, Intestinal crypts isolated from nmr*Has2* mice have significantly upregulated Has2 levels. Intestinal crypts were isolated from 5-month-old mice ($n = 4$). **d**, Intestinal crypts from old nmr*Has2* mice form more intestinal organoids in vitro. $n = 3$. Addition of HMM-HA, but not LMM-HA, to *creER* crypts resulted in a higher number of organoids. Scale bar, 100 µm. **e**, Organoid quantification in 7- and 24-month-old mice ($n = 3$). **f**, Model for the anti-ageing effects of HMM-HA. HMM-HA produced by overexpression of the nmr*Has2* gene protects tissues from oxidative stress, improves maintenance of ISCs to provide a better gut barrier function during ageing and reduces the production of pro-inflammatory molecules by immune cells. The beneficial effects of HMM-HA further contribute to the longevity and healthspan of the mice. For **b**, **c** and **e**, *P* values were calculated using two-tailed unpaired *t*-tests; *P* values are indicated in the graphs. For **b**, **c** and **e**, data are mean ± s.e.m. The symbols represent biological replicates. Adjustments were made for multiple comparisons.

both BMDMs and macrophage cell lines (Extended Data Fig. 8g–i). The elevation of HA levels after LPS challenge could be attributed to the decline in hyaluronidase (HYAL) expression. Moreover, the LPS-treated medium derived from HAS2-overexpressing macrophages exhibited a substantial accumulation of HMM-HA (Extended Data Fig. 8j,k). As a consequence, the accumulation of HMM-HA produced by HAS2 during macrophage activation probably accounts for the anti-inflammatory effects.

To test this effect in vivo, young mice were injected intraperitoneally with a low dose of LPS. Male mice had a stronger response compared with female mice as evidenced by the higher level of plasma TNF 4 h after the treatment (Fig. 5h and Extended Data Fig. 9a). Consistent with the in vitro results, both male and female nmr*Has2* mice showed reduced plasma TNF levels 4 h after LPS injection (Fig. 5h and Extended Data Fig. 9a). Female nmr*Has2* mice had lower levels of plasma TNF 24 h after the injection (Extended Data Fig. 9a). Moreover, both male and female nmr*Has2* mice produced less IL-6 in the plasma 4 h after LPS treatment (Fig. 5i and Extended Data Fig. 9b). We observed reduced inflammation in multiple tissues of female nmr*Has2* mice 24 h after injection. The liver, spleen and kidneys from female nmr*Has2* mice showed significantly lower pro-inflammatory *Il1b* and *Tnf* mRNA levels, but similar *Il6* mRNA levels (Extended Data Fig. 9c–e). These results indicate that HMM-HA suppresses the pro-inflammatory response of nmr*Has2* mice both in vitro and in vivo, contributing to reduced inflammation in old nmr*Has2* mice.

HMM-HA protects cells from oxidative stress[13]. Primary fibroblasts from nmr*Has2* mice produced more abundant hyaluronan (Extended Data Fig. 9f,g). Consistently, nmr*Has2* cells showed higher survival after H_2O_2 treatment, indicating the protective effect of HMM-HA against oxidative stress (Fig. 5j and Extended Data Fig. 9h). To test that the protective effect is conferred by HMM-HA and not by another function of nmr*Has2* gene, we generated a mouse-*Has2*-overexpressing fibroblast cell line. Overexpression of mouse *Has2* also resulted in an increased production of HMM-HA, similar to nmr*Has2*, and also exhibited a similar protective effect against oxidative stress (Extended Data Fig. 10a–c). As oxidative stress is linked to inflammation, we hypothesize that there is an additional pathway by which HMM-HA counteracts inflammation through reducing oxidative stress.

HMM-HA preserves intestinal health during ageing

Disruption of the gut barrier in older individuals contributes to chronic inflammation during ageing and promotes age-related diseases[36,37]. We compared the gut barrier function of nmr*Has2* and control mice.

The gut permeability increased with age in *creER* mice as measured by the gut to blood transfer of FITC–dextran signal. Notably, gut permeability remained unchanged between the old and young nmr*Has2* mice (Fig. 6a). Transcriptome analysis of the small intestine from young and old mice showed that the nmr*Has2* mouse transcriptome is shifted towards the younger state (Fig. 6b), with reduced inflammation during ageing in nmr*Has2* mice of both sexes (Fig. 6c).

The intestinal epithelium contributes to the maintenance of intestinal barrier function. Loss of functional epithelial cells leads to a leaky gut[38]. The mucus layer secreted by goblet cells provides a physical barrier preventing interactions between gut bacteria and intestinal epithelial cells. Notably, both young and old nmr*Has2* mice had more goblet cells in their small intestine and colon compared with the age-matched *creER* control mice (Fig. 6e–h). Paneth cells secrete antibacterial peptides, which provide a chemical barrier in the small intestine[39]. Paneth cell number increased with age in both nmr*Has2* and *creER* mice, which is believed to be an adaptive response to age-associated gut dysbiosis[40]. Interestingly, young nmr*Has2* mice had more Paneth cells compared with the young control mice and displayed a lower relative increase in the Paneth cell number with age (Fig. 6i,j). The smaller age-related increase in the Paneth cell number in nmr*Has2* mice may be due to improved intestinal health.

Intestinal stem cells (ISCs) located in the crypts give rise to the goblet cells, Paneth cells and absorptive enterocytes. The loss of functional ISCs during ageing is an important contributor to age-associated gut dysbiosis[41]. nmr*Has2* and control mice had similar numbers of ISCs in young age and old age (Fig. 7a,b). However, we observed higher expression of WNT- and Notch-pathway-related genes in the intestines of old nmr*Has2* mice, suggesting better stem cell maintenance (Extended Data Fig. 11a). Consistent with this, crypts from old *creER* mice formed far fewer organoids compared with the crypts from young *creER* and nmr*Has2* mice. Notably, the crypts isolated from nmr*Has2* mice showed strong expression of *Has2* (Fig. 7c), and the ability of those crypts to form organoids did not decrease with age (Fig. 7d,e). To test whether the improved stemness of ISCs in nmr*Has2* mice was due to hyaluronan, we added HMM-HA or LMM-HA into the Matrigel used to culture organoids. Supplying HMM-HA was sufficient to reactivate ISCs from old *creER* mice and resulted in a higher number of organoids (Fig. 7e,f). This result indicates that HMM-HA produced by nmrHas2 helps to maintain the stemness of ISCs during ageing.

The gut microbiome undergoes changes during ageing and gut dysbiosis can further contribute to systemic inflammation[42]. We compared the microbial composition between 7- and 24-month-old nmr*Has2* and control mice. At the phylum level, the operational taxonomic units (OTUs) showed that both young and old nmr*Has2* mice had increased Bacteroidetes and decreased Firmicutes levels compared with the age-matched control mice. However, only the old groups reached statistical significance (Extended Data Fig. 11b,c). A decrease in the ratio of Bacteroidetes to Firmicutes was shown to correlate with gut dysbiosis in hypertension and metabolic disorders[43,44]. At the family level, Deferribacteraceae, Streptococcaceae and Lachnospiraceae, which are known to positively correlate with inflammation, showed higher abundance in old *creER* mice. Muribaculaceae, which was linked to longevity of Spalax leucodon[45], was found at higher levels in old nmr*Has2* mice (Extended Data Fig. 11d,e). Collectively, our results indicate that old nmr*Has2* mice have improved intestinal health, contributing to reduced age-related inflammation.

Discussion

Our results demonstrate that HMM-HA produced by the nmr*Has2* gene extends the lifespan and improves the healthspan of mice by ameliorating age-related inflammation. This is achieved by directly suppressing the production of pro-inflammatory factors by immune cells, and by promoting stemness of ISCs preventing age-related decline in the intestinal barrier (Fig. 7f). These findings demonstrate that evolutionary adaptations found in long-lived species such as the naked mole-rat can be exported and adapted to benefit human health. Moreover, these findings underscore the use of HMM-HA for treating age-related inflammation in the intestine and other tissues (further discussion is provided in the Supplementary Discussion).

Online content

Any methods, additional references, Nature Portfolio reporting summaries, source data, extended data, supplementary information, acknowledgements, peer review information; details of author contributions and competing interests; and statements of data and code availability are available at https://doi.org/10.1038/s41586-023-06463-0.

1. Seluanov, A. et al. Hypersensitivity to contact inhibition provides a clue to cancer resistance of naked mole-rat. *Proc. Natl Acad. Sci. USA* **106**, 19352–19357 (2009).
2. Tian, X. et al. High-molecular-mass hyaluronan mediates the cancer resistance of the naked mole rat. *Nature* **499**, 346–349 (2013).
3. Lewis, K. N. & Buffenstein, R. in *Handbook of the Biology of Aging* (eds Kaeberlein, M. R. & Martin, G. M.) 179–204 (Elsevier, 2016).
4. Buffenstein, R. Negligible senescence in the longest living rodent, the naked mole-rat: insights from a successfully aging species. *J. Comp. Physiol. B* **178**, 439–445 (2008).
5. O'Connor, T. P., Lee, A., Jarvis, J. U. & Buffenstein, R. Prolonged longevity in naked mole-rats: age-related changes in metabolism, body composition and gastrointestinal function. *Comp. Biochem. Physiol. A* **133**, 835–842 (2002).
6. Weissmann, B. & Meyer, K. The structure of hyalobiuronic acid and of hyaluronic acid from umbilical Cord. *J. Am. Chem. Soc.* **76**, 1753–1757 (1954).
7. Fennouri, A. et al. Single molecule detection of glycosaminoglycan hyaluronic acid oligosaccharides and depolymerization enzyme activity using a protein nanopore. *ACS Nano* **6**, 9672–9678 (2012).
8. Jiang, D., Liang, J. & Noble, P. W. Hyaluronan as an immune regulator in human diseases. *Physiol. Rev.* **91**, 221–264 (2011).
9. Cyphert, J. M., Trempus, C. S. & Garantziotis, S. Size matters: molecular weight specificity of hyaluronan effects in cell biology. *Int. J. Cell Biol.* **2015**, 563818 (2015).
10. Wu, M. et al. A novel role of low molecular weight hyaluronan in breast cancer metastasis. *FASEB J.* **29**, 1290–1298 (2015).
11. Zhang, G. et al. Colorectal cancer-associated ~6 kDa hyaluronan serves as a novel biomarker for cancer progression and metastasis. *FEBS J.* **286**, 3148–3163 (2019).
12. Ruppert, S., Hawn, T., Arrigoni, A., Wight, T. & Bollyky, P. Tissue integrity signals communicated by high-molecular weight hyaluronan and the resolution of inflammation. *Immunol. Res.* **58**, 186–192 (2014).
13. Strachan, R. K., Smith, P. & Gardner, D. L. Hyaluronate in rheumatology and orthopaedics: is there a role?. *Ann. Rheum. Dis.* **49**, 949–952 (1990).
14. Muto, J., Yamasaki, K., Taylor, K. R. & Gallo, R. L. Engagement of CD44 by hyaluronan suppresses TLR4 signaling and the septic response to LPS. *Mol. Immunol.* **47**, 449–456 (2009).
15. Šoltés, L. et al. Degradative action of reactive oxygen species on hyaluronan. *Biomacromolecules* **7**, 659–668 (2006).
16. Takasugi, M. et al. Naked mole-rat very-high-molecular-mass hyaluronan exhibits superior cytoprotective properties. *Nat. Commun.* **11**, 2376 (2020).
17. Garantziotis, S. & Savani, R. C. Hyaluronan biology: a complex balancing act of structure, function, location and context. *Matrix Biol.* **78**, 1–10 (2019).
18. Ferrucci, L. & Fabbri, E. Inflammageing: chronic inflammation in ageing, cardiovascular disease, and frailty. *Nat. Rev. Cardiol.* **15**, 505–522 (2018).
19. Franceschi, C. & Campisi, J. Chronic inflammation (inflammaging) and its potential contribution to age-associated diseases. *J. Gerontol. A* **69**, S4–S9 (2014).
20. Fraser, J. & Laurent, T. The biology of hyaluronan. *Ciba Found. Symp.* **143**, 41–59 (1989).
21. Ward, J. M. Lymphomas and leukemias in mice. *Exp. Toxicol. Pathol.* **57**, 377–381 (2006).
22. Horvath, S. et al. DNA methylation clocks tick in naked mole rats but queens age more slowly than nonbreeders. *Nat. Aging* **2**, 46–59 (2022).
23. Arneson, A. et al. A mammalian methylation array for profiling methylation levels at conserved sequences. *Nat. Commun.* **13**, 783 (2022).
24. Mozhui, K. et al. Genetic loci and metabolic states associated with murine epigenetic aging. *eLife* **11**, e75244 (2022).
25. Whitehead, J. C. et al. A clinical frailty index in aging mice: comparisons with frailty index data in humans. *J. Gerontol. A* **69**, 621–632 (2014).
26. Shiotsuki, H. et al. A rotarod test for evaluation of motor skill learning. *J. Neurosci. Methods* **189**, 180–185 (2010).
27. Maddatu, T. P., Grubb, S. C., Bult, C. J. & Bogue, M. A. Mouse Phenome Database (MPD). *Nucleic Acids Res.* **40**, D887–D894 (2012).
28. Chen, H., Zhou, X., Shoumura, S., Emura, S. & Bunai, Y. Age-and gender-dependent changes in three-dimensional microstructure of cortical and trabecular bone at the human femoral neck. *Osteoporos. Int.* **21**, 627–636 (2010).
29. Tyshkovskiy, A. et al. Identification and application of gene expression signatures associated with lifespan extension. *Cell Metab.* **30**, 573–593 (2019).
30. Tyshkovskiy, A. et al. Distinct longevity mechanisms across and within species and their association with aging. *Cell* **186**, 2929–2949 (2023).
31. Schaum, N. et al. Ageing hallmarks exhibit organ-specific temporal signatures. *Nature* **583**, 596–602 (2020).
32. Lu, J. Y. et al. Comparative transcriptomics reveals circadian and pluripotency networks as two pillars of longevity regulation. *Cell Metab.* **34**, 836–856 (2022).

33. Gubbels Bupp, M. R., Potluri, T., Fink, A. L. & Klein, S. L. The confluence of sex hormones and aging on immunity. *Front. Immunol.* **9**, 01269 (2018).
34. Litwiniuk, M., Krejner, A., Speyrer, M. S., Gauto, A. R. & Grzela, T. Hyaluronic acid in inflammation and tissue regeneration. *Wounds* **28**, 78–88 (2016).
35. Rayahin, J. E., Buhrman, J. S., Zhang, Y., Koh, T. J. & Gemeinhart, R. A. High and low molecular weight hyaluronic acid differentially influence macrophage activation. *ACS Biomater. Sci. Eng.* **1**, 481–493 (2015).
36. Biragyn, A. & Ferrucci, L. Gut dysbiosis: a potential link between increased cancer risk in ageing and inflammaging. *Lancet Oncol.* **19**, e295–e304 (2018).
37. Thevaranjan, N. et al. Age-associated microbial dysbiosis promotes intestinal permeability, systemic inflammation, and macrophage dysfunction. *Cell Host Microbe* **21**, 455–466 (2017).
38. Sovran, B. et al. Age-associated impairment of the mucus barrier function is associated with profound changes in microbiota and immunity. *Sci. Rep.* **9**, 1437 (2019).
39. Bevins, C. L. & Salzman, N. H. Paneth cells, antimicrobial peptides and maintenance of intestinal homeostasis. *Nat. Rev. Microbiol.* **9**, 356–368 (2011).
40. Moorefield, E. C. et al. Aging effects on intestinal homeostasis associated with expansion and dysfunction of intestinal epithelial stem cells. *Aging* **9**, 1898 (2017).
41. Funk, M. C., Zhou, J. & Boutros, M. Ageing, metabolism and the intestine. *EMBO Rep.* **21**, e50047 (2020).
42. DeJong, E. N., Surette, M. G. & Bowdish, D. M. The gut microbiota and unhealthy aging: disentangling cause from consequence. *Cell Host Microbe* **28**, 180–189 (2020).
43. Yang, T. et al. Gut dysbiosis is linked to hypertension. *Hypertension* **65**, 1331–1340 (2015).
44. Ley, R. E., Turnbaugh, P. J., Klein, S. & Gordon, J. I. Human gut microbes associated with obesity. *Nature* **444**, 1022–1023 (2006).
45. Sibai, M. et al. Microbiome and longevity: high abundance of longevity-linked Muribaculaceae in the gut of the long-living rodent spalax leucodon. *OMICS* **24**, 592–601 (2020).

Methods

Animal husbandry

All animal experiments were approved and performed in accordance with guidelines set forth by the University of Rochester Committee on Animal Resources (protocol number 2017-033, mouse). Mice were group housed in IVC cages (up to 5 animals per cage) in a specific-pathogen-free environment and fed standard chow diet (Altromin 1324; total pathogen free, irradiated with 25 kGy) and water ad libitum. Animal rooms were maintained at 21–24 °C and 35–75% relative humidity, under a 12 h–12 h (06:00 to 18:00) dark–light cycle. Cages were routinely replaced every 10–14 days.

Mice and lifespan study

C57BL/6 mice were obtained from Charles River Labs, *R26-creER*^{T2} mice were obtained from JAX. To generate nmr*Has2* conditional transgenic mice, the nmr*Has2* coding sequence was subcloned into the pCALNL-GFP plasmid (Addgene plasmid, 13770) to replace GFP. Transgenic mice were made by UC-Irvine Transgenic Mouse Facility. nmr*Has2* and control *creER* mice were obtained by crossing mice heterozygous for the nmr*Has2* gene with homozygous *R26-creER*^{T2} mice. At the age of 1 month, progenies were separated by sex, ear tagged and the distal tail (~2 mm) was cut for genotyping determination. All mice received 80 mg per kg tamoxifen at 3 months of age for 5 consecutive days. *creER* and nmr*Has2* mice were housed in the same cage for all of the experiments. None of the animals entered into the ageing study were allowed to breed. Mice were inspected daily for health issues, and any death was recorded. Animals showing significant signs of morbidity, based on the AAALAC guidelines, were euthanized for humane reasons and were used for lifespan analysis as they were deemed to have lived to their full lifespan. No mice were censored from the analysis. Lifespan was analysed by Kaplan–Meier survival curves, and *P* values were calculated using log-rank tests in GraphPad Prism.

Necropsy

Cages were inspected every night. Dead animals were removed from cages, opened and examined macroscopically by a trained person. A fraction of the animals could not be examined because they were too decomposed or disturbed by other animals. Organs were moved, turned or lifted with forceps for the examination but were not removed. All visible tumours, as well as any other observations were noted.

Tissue and plasma collection

Animals were brought to the laboratory in their holding cages and euthanized one by one for dissection. Mice were euthanized by isofluorane anaesthesia followed by cervical dislocation. The dissection was performed as rapidly as possible following euthanasia by several trained staff members working in concert on one mouse. Tissue samples were either rapidly frozen in liquid nitrogen (for HA amount and molecular mass determination and RNA-seq) or fixed in 4% formalin (for histology). Blood was collected by cardiac puncture into EDTA-coated tubes, centrifuged and the plasma was aliquoted and rapidly frozen in liquid nitrogen. All frozen samples were stored at −80 °C.

HA preparation

For purifying HA from tissues, 200 mg of pulverized tissue from 5-month-old mice was mixed with proteinase K solution (final concentrations of 1 mM Tris-Cl pH 8.0, 2.5 mM EDTA, 10 mM NaCl, 0.05% SDS, 2 mg ml^{-1} proteinase K), and incubated at 55 °C overnight followed by saturated phenol–chloroform–isoamyl alcohol (Sigma-Aldrich) extraction. HA was precipitated with isopropanol and centrifugation (12,000*g* for 15 min) then washed with 70% ethanol (12,000*g* for 10 min) and dissolved in 600 µl 10 mM Tris buffer at pH 8 overnight at room temperature. The purified HA was digested with SuperNuclease (final concentration of 50 U ml^{-1}, Lucerna-chem) overnight at 37 °C to eliminate nucleic acid contamination. HA was extracted by saturated phenol–chloroform–isoamyl alcohol (Sigma-Aldrich), precipitated by isopropanol and washed with 70% ethanol again. The pellet was dissolved in 30 µl 10 mM Tris buffer at pH 8 overnight at room temperature.

For HA purification from medium, conditioned media were first mixed with proteinase K solution (final concentrations of 1 mM Tris-Cl pH 8.0, 2.5 mM EDTA, 10 mM NaCl, 0.05% SDS, 1 mg ml^{-1} proteinase K) and incubated at 55 °C for 4 h. After protein digestion, media were extracted with saturated phenol–chloroform–isoamyl alcohol (Sigma-Aldrich). HA was precipitated with ethanol and centrifugation (4,000*g* for 45 min). HA pellet was dissolved in PBS and then extracted with 1/100 volume of Triton X-114. After Triton X-114 extraction, HA was precipitated again with ethanol. Finally, the HA pellet was washed with 70% ethanol and dissolved in PBS.

Pulse-field gel electrophoresis

Purified HA was mixed with sucrose solution (final concentration of 333 mM) and loaded onto a 0.4% SeaKem Gold agarose gel (Lonza). HA-Ladders (Hyalose) were run alongside the samples. The samples were run for 16 h at 9 °C at 4 V with a 1–10 running ratio in TBE buffer using CHEF-DRII system (Bio-Rad). After the run, the gel was stained with 0.005% (w/v) Stains-All (Santa Cruz) in 50% ethanol overnight. The gel was then washed twice with 10% ethanol for 12 h, exposed to light to decrease background and photographed with ChemiDoc Imaging System (Bio-Rad).

HA ELISA

Hyaluronan concentration in the medium was quantified using the hyaluronan ELISA kit (R&D systems) according to the manufacturer's instructions.

Rotarod performance

Motor performance was assessed using the protocol described previously[46]. In brief, gross motor control was measured using the rotarod (IITC Life Science). For this test, each mouse was placed onto a cylindrical dowel (diameter, 95.525 mm) raised around 30 cm above the floor of a landing platform. Mice were placed onto the dowels for 3 min to allow them to acclimatize to the test apparatus. Once initiated, the cylindrical dowels began rotating and accelerated from 5 rpm to a final speed of 20 rpm over 60 s. During this time, the mice were required to walk in a forward direction on the rotating dowels for as long as possible. When the mice were no longer able to walk on the rotating dowels, they fell onto the landing platform below. This triggered the end of the trial for an animal and measurements of time to fall were collected. Passive rotations where mice clung to and consequently rotated with the dowel were also used to define the end of the trial. The mice were then returned to their cages with access to food and water for 10 min. This procedure was repeated for a total of six trials, with the first three trials used for training and subsequent trials used for data analysis.

Forelimb grip strength

The forelimb grip strength of mice was measured using a grip strength meter (Columbus Instrument). Mice were held by the base of the tail close to the horizontal bar to allow them to reach and grab onto the bar with their forelimbs. The mice were then positioned such that their body was horizontal and in line with the bar. They were then pulled horizontally away from the bar by the tail until their grip was released. The tension was measured and defined as grip strength. The mice were given 1 min intertrial intervals during which they were returned to their cages with access to food and water. This procedure was repeated for a total of nine trials for each mouse (with the mean value of nine trials used for analysis).

Frailty index assessment

The frailty index was assessed as described previously[25]. In brief, 31 health-related deficits were assessed for each mouse. A mouse was weighed, and the body surface temperature was measured three times with an infrared thermometer (Thermo Fisher Scientific). Body weight and temperature were scored on the basis of their deviation from the mean weight and temperature of young mice[25]. A total of 29 other items across the integument, physical/musculoskeletal, ocular/nasal, digestive/urogenital and respiratory systems were scored as 0, 0.5 and 1 on the basis of the severity of the deficit. The total score across the items was divided by the number of items measured to give a frailty index score of between 0 and 1.

Micro-CT scan

Both femurs and tibia of the mice were analysed at a micro computed tomography (micro-CT) facility (Tissue Imaging (BBMTI) Core in the Center for Musculoskeletal Research, University of Rochester). Micro-CT was performed with a state-of-the-art scanner (VivaCT 40, Scanco USA) for live small animals and specimens, without contrast agents. The scanner was fitted with an adjustable X Ray Source Energy (30–70 kVp) and scan (using Scancocone beam geometry) specimens in a field of view of up to 39 mm and a scan length of 145 mm at a nominal resolution of 10 μm. Scan acquisition, reconstruction, analysis and measurements were performed using a specialized suite of 64 bit software applications running on an open VMS platform.

The relevant 3D images were imported after processing into the scan software and the parameters such as bone mass density, bone volume/tissue volume, bone surface/bone volume, bone surface/total volume, trabecular number, trabecular separation and connectivity density were measured.

Methylation clock

Genomic DNA from the livers of 24-month-old *creER* and nmr*Has2* mice was purified using the DNeasy Blood & Tissue Kit (Qiagen). A total of 100 ng of purified genomic DNA was used for the methylation measurement. All DNA methylation data used were generated using the custom Illumina chip HorvathMammalMethylChip40—the mammalian methylation array. The particular subset of species for each probe is provided in the chip manifest file can be found at NCBI Gene Expression Omnibus (GEO; GPL28271). The SeSaMe normalization method was used to define β values for each probe[47]. The methylation age was normalized to chronological age to calculate the age acceleration value.

To investigate the CpG sites that drive the epigenetic age difference between experimental and control groups, we tested the methylation levels of CpG sites reported to change during mouse ageing in a previous study[24]. Paired Student's *t*-tests were used to calculate the statistical significance.

DMBA and TPA treatment

A total of 13 young *creER* and 11 age-matched young nmr*Has2* mice were topically treated with 7,12-dimethylbenz(a)anthracene and 12-*O*-tetradecanoylphorbol-13-acetate (DMBA and TPA). A single dose of DMBA (7.8 mM dissolved in acetone) was topically treated to mice on the dorsal trunk. Then, 3 days after, 0.4 mM of TPA was treated 3 times per week. The formation of papilloma was quantified 20 weeks after TPA treatment.

Measurement of cytokines and chemokines in the plasma

A total of 36 cytokines and chemokines were measured in the plasma of young and old mice using the Luminex multiplex technique using the Cytokine & Chemokine 36-Plex Mouse ProcartaPlex Panel 1A kit (Thermo Fisher Scientific). The Luminex multiplex assay was performed using undiluted plasma samples according to the manufacturer's instructions.

Tissue sectioning, immunofluorescence and RNAscope in situ hybridization

Paraffin-embedded specimens were sectioned at a thickness of 10 μm. Tissue sections were deparaffinized with xylene and dehydrated in a descending alcohol series of 100, 95, 80, 70 and 50%. These initial processing steps were the same for all the staining procedures described below and all staining procedures were performed on the same samples; the samples were rehydrated in PBS for 30 min before performing immunofluorescence. For antibody-based assays, the sections were incubated twice in antigen-retrieval buffer (0.1 M sodium citrate, 0.1 M citric acid, pH 6.0) for 15 min at 90–100 °C before blocking. All of the slides were blocked in TBS-T, containing 5% FBS and 1% BSA, for 2 h at room temperature. Subsequently, the sections were incubated overnight at 4 °C with the following primary antibodies: anti-mUC2 (1:1,500, GeneTex) and anti-lyzozyme (1:500, Abcam). After incubation with primary antibodies, the slides were washed three times in PBS-T and incubated with goat anti-rabbit IgG (H+L) secondary antibodies conjugated with Alexa Fluor 568 (1:1,000, Invitrogen) for 1 h at room temperature. After washing five times, the slides were stained with DAPI (BioLegend) for 1 min at room temperature, mounted with mounting medium (Vector Laboratories) and observed under the confocal microscope at ×40 magnification.

For HABP staining, after deparaffinization, the slides were rehydrated in PBS for 30 min at room temperature then blocked in TBS-T, containing 5% FBS and 1% BSA, for 2 h at room temperature. All of the slides were then incubated with biotinylated hyaluronan-binding protein (1:100 for small intestine and 1:200 for other tissues, Amsbio) overnight at 4 °C. After the HABP incubation, the slides were washed and incubated with Streptavidin conjugated with Alexa Fluor 647(1:500, Thermo Fisher Scientific) for 1 h at room temperature. The slides were then washed, counterstained with DAPI, mounted and observed under the confocal microscope at ×40 magnification. At least three random fields of each sample were captured for quantification of fluorescence signals. The average intensities of HA signals were quantified using ImageJ. The experiment was repeated from at least three animals of each group to confirm the reproducibility.

The RNAscope assay was performed using the RNAscope Multiplex Fluorescent Detection Kit v2 according to the manufacturer's protocol. All of the images were acquired under the confocal microscope at ×40 magnification.

Preparation of RNA for RT–qPCR and RNA-seq

All frozen tissues were pulverized using the cell crusher. For preparing RNA from tissues, pulverized frozen tissues in the range of 10–15 mg were removed from the samples kept at −80 °C and extracted using Trizol reagent according to the supplier's instructions. After recovery of total RNA from the Trizol reagent by isopropanol precipitation, RNA was digested with DNase I for 30 min at room temperature and further purified using the RNeasy plus mini kit according to the manufacturer's instructions. For purifying RNA from cells, the RNeasy plus mini kit was used according to the user manual. The yield and quality were checked using the Nano Drop.

RT–qPCR

For quantitative PCR with reverse transcription (RT–qPCR), around 300 ng of purified RNA was reverse-transcribed into cDNA in 20 μl using the iScript cDNA synthesis kit (Bio-Rad). A total of 2 μl of this reaction was used for subsequent qPCR reactions, which were performed using SYBR green system (Bio-Rad). A list of the primer sequences is provided in Supplementary Table 1. The *Actb* gene was used as the internal normalization control.

RNA-seq

The RNA samples were processed using the Illumina TruSeq Stranded Total RNA RiboZero Gold kit and then subjected to Illumina HiSeq 4000

single-end 150 bp sequencing at New York University Genome Technology Center. Over 50 million reads per sample were obtained. The RNA-seq experiment was performed in three biological replicates for all tissues.

The RNA-seq reads were first processed using Trim_Galore (v.0.6.6), which trimmed both adapter sequences and low-quality base calls (Phred quality score < 20). The clean RNA-seq reads were used to quantify the gene expression with Salmon (v.1.4.0)[48]. Specific parameters (--useVBOpt --seqBias --gcBias) were set for sequence-specific bias correction and fragment GC bias correction. Gencode[49] (v.M25) was used for the genome-wide annotation of the gene in the mouse. The reads counts for genes were used as the input for differential expression analysis by DESeq2 (ref. 50). Low-expression genes with read counts of less than 10 were excluded. The cut-off *P* value and fold change is shown in the figure or figure legend.

For the hierarchical clustering analysis, we reanalysed published gene expression data of mice treated with rapamycin, calorie restriction, growth hormone receptor knockout. To minimize the potential batch effect, we directly compared the gene expression data of mice with intervention treatments with their corresponding control. Fold changes (intervention/control) in gene expression levels were calculated for each gene. $\log_2$-scaled fold changes in gene expression were used to perform the analysis.

GSEA[51] was performed using the Preranked model (v.4.1.0). All genes were preranked by the values of $-\log_{10}$[adjusted *P*] × (fold change)/abs(fold change). Adjusted *P* values and fold changes were obtained from DEseq2. The normalization mode was set to meandiv. Only those gene sets with a size more than 15 genes were retained for the further analysis.

GO analyses were performed using the R package clusterProfiler (release v.3.14)[52]. GO comprises three orthogonal ontologies, that is, molecular function, biological process and cellular component. All of the *P* values were adjusted using Benjamini–Hochberg correction.

Association of gene expression log-transformed fold changes induced by nmr*Has2* expression in mouse livers with previously established transcriptomic signatures of ageing and lifespan-extending interventions was examined as described in the previous study[29] separately for male and female mice. Used signatures of ageing included tissue-specific brain, liver and kidney signatures as well as multi-tissue signatures of mouse, rat and human. Signatures of lifespan-extending interventions included genes differentially expressed in mouse tissues in response to individual interventions, including caloric restriction, rapamycin and mutations associated with growth hormone deficiency, along with common patterns of lifespan-extending interventions and expression changes associated with the mouse maximum and median lifespan.

Pairwise Spearman correlation between log[FC] induced by nmrHas2 expression and associated with signatures of ageing and longevity was calculated on the basis of the union of the top 400 statistically significant genes (with the lowest *P* value) for each pair of signatures.

For the identification of enriched functions affected by nmr*Has2* expression in mouse livers, we performed Fisher's exact tests and functional GSEA[51] on a preranked list of genes based on $\log_{10}$[*P*] corrected by the sign of regulation, calculated as:

$$-(\mathrm{pv}) \times \mathrm{sgn}(\mathrm{lfc}),$$

where pv and lfc are *P* value and log-transformed fold change of a certain gene, respectively, obtained from the edgeR output, and sgn is the signum function (equal to 1, −1 and 0 if the value is positive, negative or equal to 0, respectively). Hallmark, KEGG and Reactome ontologies from the Molecular Signature Database (MSigDB) were used as gene sets. Fisher's exact tests and GSEA were performed separately for each sex using the gprofile2 and fgsea R packages, respectively. A *q*-value cut-off of 0.1 was used to select statistically significant functions.

Similar analysis was performed for gene expression signatures of ageing and lifespan-extending interventions. Pairwise Spearman correlation was calculated for individual signatures of nmrHas2 expression, ageing and lifespan-extending interventions based on NES estimated by GSEA. A heat map coloured by NES was built for manually chosen statistically significant functions (adjusted $P < 0.1$). A complete list of functions enriched by genes perturbed by nmr*Has2* expression in mouse livers is included in Supplementary Table 3.

Primary fibroblast isolation and cell culture

Primary skin fibroblasts were isolated from under-arm skin from 5-month-old *creER* and nmr*Has2* mice. Skin tissues were shaved and cleaned with 70% ethanol and then minced and incubated in DMEM/F-12 medium (Thermo Fisher Scientific) with Liberase (Millipore Sigma) at 37 °C on a stirrer for 40 min. Tissues were then washed and plated with DMEM/F-12 medium containing 15% fetal bovine serum (GIBCO) and antibiotic–antimycotic (GIBCO). When cells were 80% confluent, the isolated cells were frozen in liquid nitrogen within two passages. All subsequent fibroblast cultures were performed in EMEM (ATCC) supplemented with 10% fetal bovine serum (GIBCO), 100 U ml^{-1} penicillin and 100 mg ml^{-1} streptomycin (GIBCO). The Raw264.7 cell line was purchased from ATCC and maintained using DMEM (Gibco) supplemented with 10% fetal bovine serum (GIBCO), 100 U ml^{-1} penicillin and 100 mg ml^{-1} streptomycin (GIBCO). The Raw cells used for all experiments were all under passage four. All primary cells were cultured at 37 °C with 5% CO_2 and 3% O_2.

Apoptosis assay

Skin fibroblast cells under population doubling 15 were used for H_2O_2 treatment. Cells with around 80% confluency were treated with H_2O_2 at concentrations of 100 μM, 200 μM and 400 μM for 24 h. Cells were collected, and apoptotic cells were quantified using the Annexin V FLUOS Staining Kit (Roche) according to the manufacturer's instructions. After staining, cells were analysed with CytoFlex flow cytometer (Beckman). Cells that were double negative for annexin-V and PI signals were defined as live cells.

BMDM isolation, culture and LPS challenge

BMDMs were isolated from 5-months-old *creER* and nmr*Has2* mice. Mice were euthanized by cervical dislocation and the hind legs were dissected. Using aseptic technique, the bone marrow was extracted from the tibia and femur bones after removing the surrounding muscle. To do so, the joints were cut using a scalpel and the exposed bone marrow was flushed out the ends of the bones using a 27-gauge needle and a 10 ml syringe filled with cold RPMI-1640 medium. Clumps were gently disaggregated using a needle-less syringe and passed through a 70 μm cell strainer. The cell suspension was centrifuged at 250*g* for 5 min at room temperature to pellet cells. Bone marrow cells were subsequently cultured in RPMI-164 (GIBCO) supplemented with 10% fetal bovine serum (GIBCO), 100 U ml^{-1} penicillin, 100 mg ml^{-1} streptomycin (GIBCO), and 10 ng ml^{-1} recombinant mouse M-CSF (R&D) at 37 °C with 5% CO_2 and 3% O_2 on day 0. Fresh medium was changed every 48 h, a double volume of medium was used on day 4 and M-CSF was supplemented on day 6 to avoid removing the HA produced by the cells. LPS (10 ng ml^{-1}) was used to treat macrophages on day 7. Cells were collected 24 h after LPS treatment for RNA extraction.

Gut permeability assay

Tracer FITC-labelled dextran (4 kDa; Sigma-Aldrich) was used to assess in vivo intestinal permeability. Mice were deprived of food 8 h before and deprived of both food and water after an oral gavage using 200 ml of 80 mg ml^{-1} FITC-dextran. Blood was retro-orbitally collected after 4 h, and the fluorescence intensity was measured on fluorescence plates using an excitation wavelength of 493 nm and an emission wavelength of 518 nm. The untreated mouse plasma was used as a blank.

Isolation and culture of primary intestinal crypts

Around 20 cm small intestines from 7- and 18-month old mice were removed and flushed using 10 ml syringe with clear lumenal contents. The intestines were then opened longitudinally, washed in 20 ml cold PBS and cut into ~5 mm sections, and placed into the 50 ml canonical tube containing 15 ml cold PBS. Intestinal crypts were mechanically released from the lamina propria by vigorous pipetting and washed 20 times with PBS and the incubated in 25 ml gentle cell dissociation reagent (StemCell Technology) for 15 min at room temperature. The dissociation reagent was next neutralized by adding 10 ml of cold PBS containing 1% BSA. The supernatants containing crypts were filtered through a 70 μm cell strainer and centrifuged at 290*g* for 5 min at 4 °C then washed once more with cold PBS containing 1% BSA. Isolated crypts were counted and embedded in Matrigel (Corning) on ice at around 12.5 crypts per μl and mixed with the same volume of IntestiCult Organoid Growth medium (StemCell Technology). Matrigel beads occupying the centre of the well were constructed using 40 μl of Matrigel to form a solid dome-like structure in an eight-well chamber slide and were subsequently overlaid with 400 μl IntestiCult Organoid Growth medium. For the HA treatment, 20 μg ml^{-1} HMM or LMM HA (R&D) were directly added to the Matrigel crypts mixture. Primary intestinal crypts were incubated in a fully humidified culture chamber with 5% CO_2 at 37 °C. The culture medium was changed every 48 h, and the organoid-forming efficiency was calculated on day 4.

Microbiota analysis

Fresh faecal samples from 9- and 23-month-old animals were obtained in the morning, immediately snap-frozen in liquid nitrogen and stored at −80 °C. These samples were used for 16S rRNA gene analysis for microbiota profiling from the V1–V2 region of the 16S rRNA genes. DNA extraction was performed using the QIAamp DNA Stool Mini Kit (Qiagen) according to the manufacturer's instructions. DNA was eluted in 50 μl DNase-free water. A total of 20 ng of DNA was used for the amplification of the 16S rRNA gene with the primers 27F-DegS (5′-TCGTCGGCAGCGTCAGATGTGTATAAGAGACAGGTTYGATYMTGGCTCAG-3′) and 338R I (5′-GTCTCGTGGGCTCGGAGATGTGTATAAGAGACAGGCWGCCTCCCGTAGGAGT-3′) + 338R II (5′-GTCTCGTGGGCTCGGAGATGTGTATAAGAGACAGGCWGCCACCCGTAGGTGT-3′)[53] for 25 cycles. The primers have Illumina sequencing index attached; index forward (5′-TCGTCGGCAGCGTCAGATGTGTATAAGAGACAG-3′) and index reverse (5′-GTCTCGTGGGCTCGGAGATGTGTATAAGAGACAG-3′). The PCR was performed in a total volume of 50 μl containing 1× HF buffer (New England BioLabs), 1 μl dNTP Mix (New England BioLabs), 1 U of Phusion Hot Start II High-Fidelity DNA polymerase (New England BioLabs), 500 nM of the 27F-DegS primer and 500 nM of an equimolar mix of two reverse primers, 338R I and II. The size of the PCR products (~375 bp) was confirmed by gel electrophoresis using 5 μl of the amplification reaction mixture on a 1% (w/v) agarose gel. The PCR products were purified using the QIAquick PCR Purification Kit (Qiagen). The dual indices and Illumina sequencing adapters were then attached using the Nextera XT index kit (Illumina) according to manufacturer's instructions. Purified amplicon pools were 250 bp paired-end sequenced using the Illumina MiSeq system.

The Illumina MiSeq data analysis was performed using a workflow involving the Quantitative Insights Into Microbial Ecology (QIIME2) pipeline[54]. The reads were processed as follows: reads were filtered for not matching barcodes; OTU picking and chimera removal was done by matching the sequences to the Silva 111 database (with only one mismatch allowed) and a biom and, using clustalw, a multiple-sequence alignment and phylogenetic tree file was generated. Further outputs were generated using QIIME, such as filtered reads per sample, PD whole tree diversity measurements and the level 1–6 taxonomic distributions with relative abundances. A 37,000-read cut-off was used for all of the samples.

Statistical and demographic analysis

Data are shown as mean ± s.e.m. unless stated otherwise. *n* indicates the number of animals per test group; age and sex are also noted. The number of animals chosen for each experiment was calculated using power analysis. Randomly picked littermates were used for all of the experiments. Student's *t*-tests (unpaired, two-tailed, equal variance) were used for all pairwise comparisons that satisfied the requirement for normal distribution. Mann–Whitney *U*-tests were used for data that did not satisfy the requirements for normal distribution. All relevant *P* values are shown in the figures; NS, not significant. Demographic data were processed with GraphPad Prism software to compute the mean and median lifespans, s.e.m., percentage increase in the median and *P* values (log-rank test) for each cohort.

Reporting summary

Further information on research design is available in the Nature Portfolio Reporting Summary linked to this article.

Data availability

The RNA-seq data, epigenetic clock data and 16S rDNA sequencing data produced in this paper have been deposited at the GEO (GSE234563, GSE234154, GSE234286).

46. Tung, V. W., Burton, T. J., Dababneh, E., Quail, S. L. & Camp, A. J. Behavioral assessment of the aging mouse vestibular system. *J. Vis. Exp.* https://doi.org/10.3791/51605 (2014).
47. Zhou, W., Triche Jr, T. J., Laird, P. W. & Shen, H. SeSAMe: reducing artifactual detection of DNA methylation by Infinium BeadChips in genomic deletions. *Nucleic Acids Res.* **46**, e123 (2018).
48. Patro, R., Duggal, G., Love, M. I., Irizarry, R. A. & Kingsford, C. Salmon provides fast and bias-aware quantification of transcript expression. *Nat. Methods* **14**, 417–419 (2017).
49. Frankish, A. et al. GENCODE reference annotation for the human and mouse genomes. *Nucleic Acids Res.* **47**, D766–D773 (2019).
50. Anders, S. & Huber, W. Differential expression analysis for sequence count data. *Genome Biol.* **11**, R106 (2010).
51. Subramanian, A. et al. Gene set enrichment analysis: a knowledge-based approach for interpreting genome-wide expression profiles. *Proc. Natl Acad. Sci. USA* **102**, 15545–15550 (2005).
52. Wu, T. et al. clusterProfiler 4.0: a universal enrichment tool for interpreting omics data. *Innovation* **2**, 100141 (2021).
53. Fransen, F. et al. β2→1-Fructans modulate the immune system in vivo in a microbiota-dependent and-independent fashion. *Front. Immunol.* **8**, 154 (2017).
54. Caporaso, J. G. et al. QIIME allows analysis of high-throughput community sequencing data. *Nat. Methods* **7**, 335–336 (2010).

Acknowledgements This work was supported by grants from the National Institutes of Health to V.N.G., A.S. and V.G.

Author contributions Z.Z., A.S. and V.G. designed research, analysed data and wrote the manuscript. Z.Z. performed most of the experiments. J.Y.L., A.T. and V.N.G. analysed RNA-seq data. X.T. designed research and generated the transgenic mouse strain. Z.Z., X.T., F.T.Z. and S.E. performed the ageing study. K.B. helped with immunofluorescence staining. J.A. performed the DMBA/TPA treatment. Q.L. helped with collecting and preparing faecal DNA for microbiome analysis. D.F. helped with the cell apoptosis assay. E.R. and S.A.B. helped with maintaining the mouse colony. S.H. performed the methylation clock assay. A.S. and V.G. supervised research.

Competing interests The authors declare no competing interests.

Additional information

Supplementary information The online version contains supplementary material available at https://doi.org/10.1038/s41586-023-06463-0.

Correspondence and requests for materials should be addressed to Andrei Seluanov or Vera Gorbunova.

Peer review information *Nature* thanks F. Dilworth and the other, anonymous, reviewer(s) for their contribution to the peer review of this work.

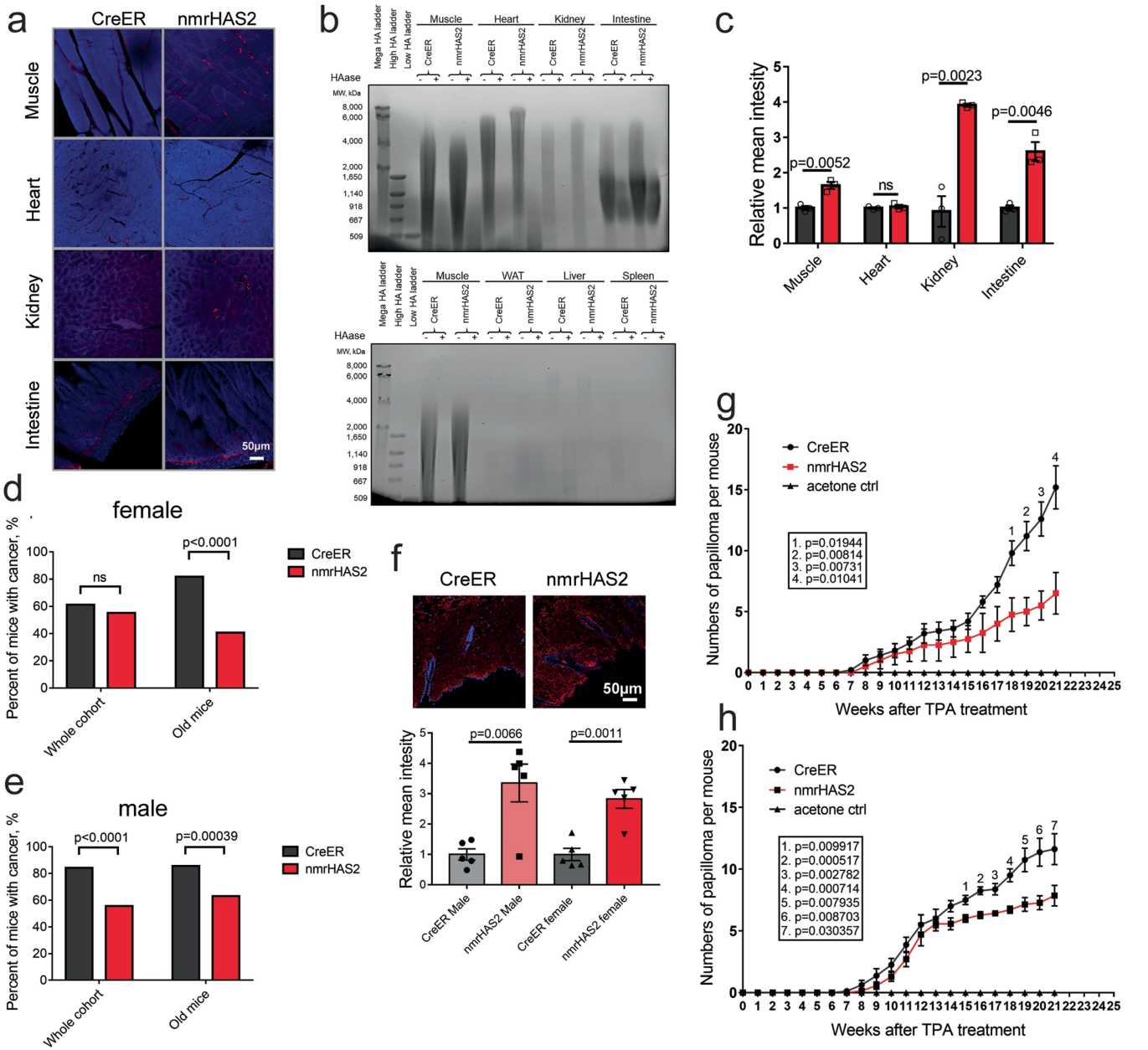

Extended Data Fig. 1 | nmrHAS2 mice exhibit resistance to spontaneous and induced cancer. a. Representative stainings of HABP staining in organs of male nmrHAS2 and CreER mice. **b**. Pulse field gel shows that male nmrHAS2 mice have higher molecular weight and more abundant hyaluronic acid than CreER control mice. HA was extracted from 200 mg of pooled tissue from two individuals. HAase treated samples were run in parallel to confirm the specificity of HA staining. **c**. Quantification of relative HABP fluorescence intensity shown in **b**. n = 3. **d**. Old female nmrHAS2 mice have much lower spontaneous cancer incidence n = 47 for CreER and n = 49 for nmrHAS2. **e**. Old male nmrHAS2 mice have much lower spontaneous cancer incidence n = 27 for CreER and n = 32 for nmrHAS2. **f**. HABP staining shows that skin of nmrHAS2 mice has higher hyaluronan levels, n = 5. **g**. Quantification of papilloma formation in DMBA/TPA treated female mice. n = 3 for acetone treated mice, n = 5 for CreER, and n = 4 for nmrHAS2. **h**. Quantification of papilloma formation in DMBA/TPA treated male mice. n = 4 for acetone treated mice, n = 8 for CreER, and n = 7 for nmrHAS2. **c,f,g**. p-values were calculated by two-tailed unpaired t-test (p-values are indicated in the graphs). Bars represent the means, error bar displays the standard error, dots represent biological replicates. **d-e**. Old mice are older than 27 months. P-values were calculated by two tailed Chi-square test.

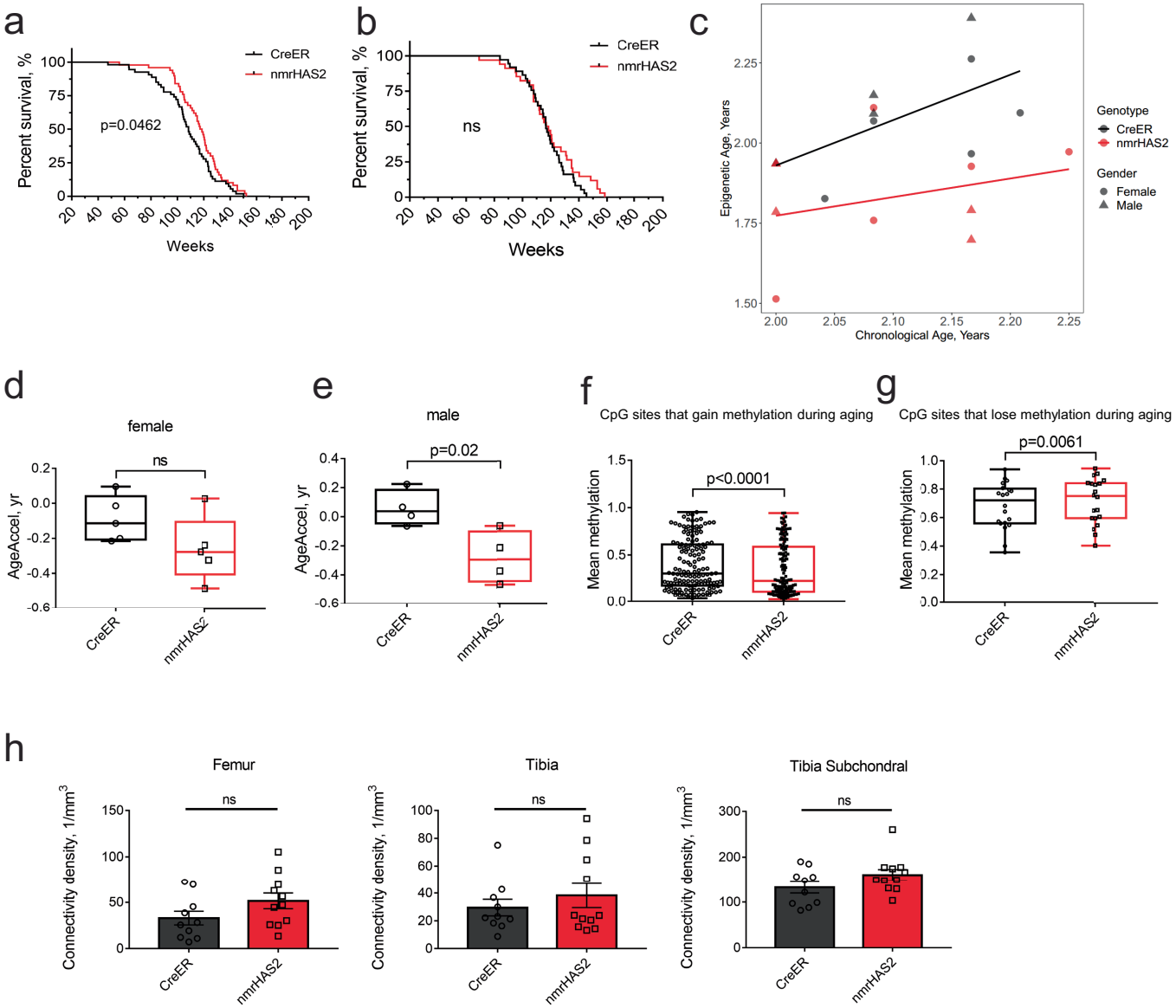

Extended Data Fig. 2 | nmrHAS2 mice show extended lifespan and healthspan. a. Female nmrHAS2 mice (n = 50) have extended median lifespan compared to female CreER mice (n = 54). p-value for median lifespan was calculated using two tailed log-rank test. **b**. Male nmrHAS2 (n = 34) mice have extended maximum lifespan compared to male CreER mice (n = 37). p-value for median lifespan was calculated using two tailed log-rank test. **c**. Old nmrHAS2 mice display younger epigenetic age. **d**-**e**. Old nmrHAS2 female mice (**d**) and old nmrHAS2 male mice (**e**) display lower age acceleration, or younger biological age than CreER controls. **f**. Mean methylation level of CpG sites that gain methylation during aging. Analysis was performed based on 9 animals. **g**. Mean methylation level of CpG sites that lose methylation during aging. Analysis was performed based on 9 animals. **h**. Old male nmrHAS2 mice (n = 11) have the same level of bone connectivity density compared to age-matched controls (n = 10). p-values were calculated by two-tailed unpaired t-test (p-values are indicated in the graphs). Bars represent the means, error bars show standard errors, dots represent biological replicates. **d, e**. The five-number summary on the boxplot displays the minimum, first quartile, median, third quartile, and maximum. p-values were calculated by two-tailed unpaired t-test. **f, g**. The five-number summary on the boxplot displays the minimum, first quartile, median, third quartile, and maximum. p-values were calculated by two-tailed paired t-test.

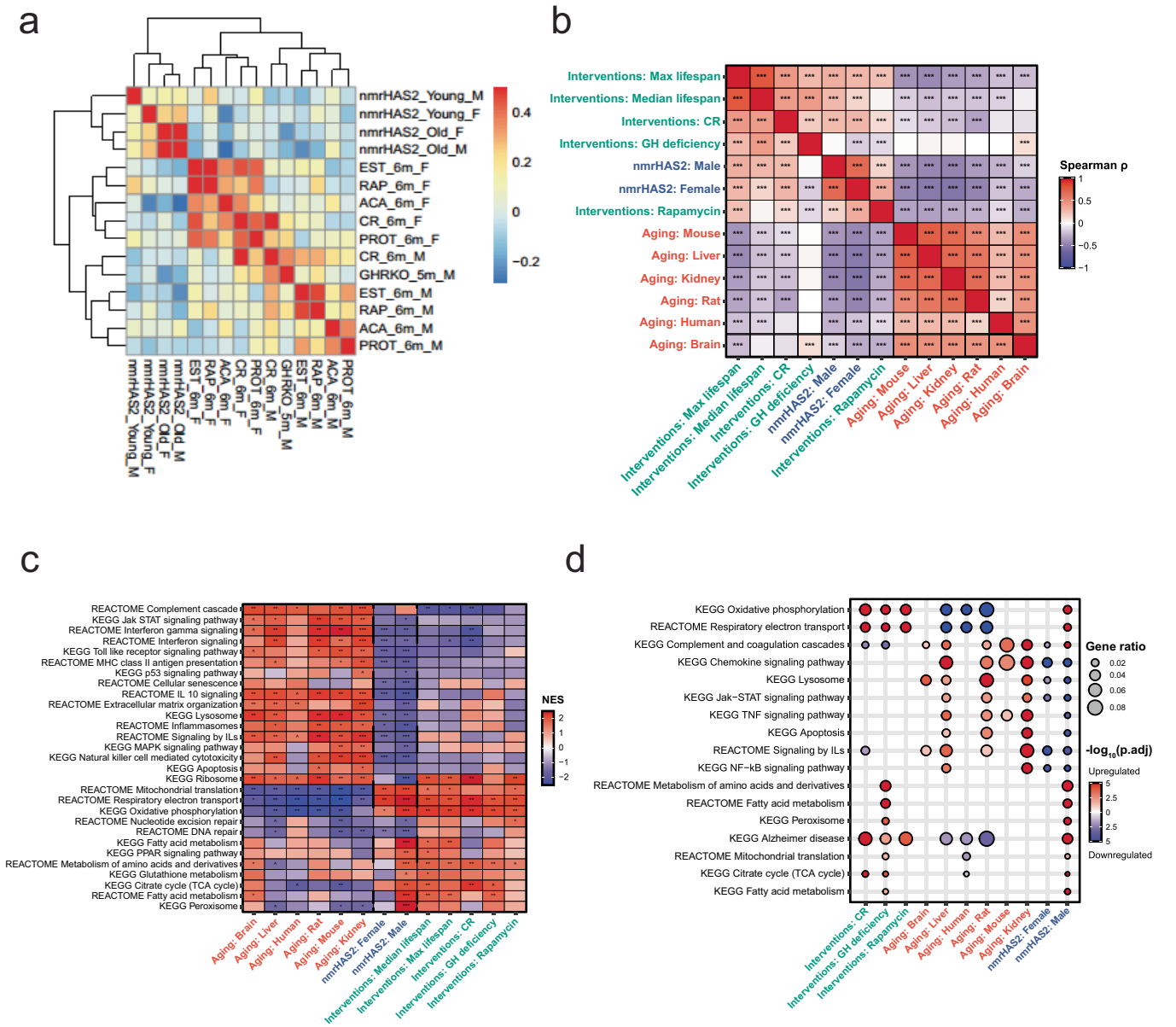

Extended Data Fig. 3 | nmrHAS2 mice showed a distinct transcriptomic signature. a. nmrHAS2 mice display an expression signature distinct form mice subjected to other pro-longevity interventions. A heatmap of correlation analysis performed on liver whole transcriptomes. **b**. Association between nmrHAS2 effect and signatures of lifespan-extending interventions and mammalian aging based on functional enrichment (GSEA) scores. Only functions enriched by at least one signature (adjusted p-value < 0.1) were used for the calculation. Exact adjusted p-values are shown in Extended Data Table 2. **c**. Functional enrichment (GSEA) of gene expression signatures associated with nmrHAS2, mammalian aging and established lifespan-extending interventions. Only functions significantly enriched by at least one signature (adjusted p-value < 0.1) are presented. Exact adjusted p-values are shown in Supplementary Table 4. **d**. Functional enrichment (Fisher exact test) of genes significantly associated with the effect of nmrHAS2, mammalian aging and established lifespan-extending interventions. Only functions enriched by at least one aggregated signature (adjusted p-value < 0.1) are shown. Proportion of pathway-associated genes is reflected by bubble size. Exact adjusted p-values are shown in Supplementary Table 5. **b-d**. ^ p.adjusted < 0.1; * p.adjusted < 0.05; ** p.adjusted < 0.01; *** p.adjusted < 0.001.

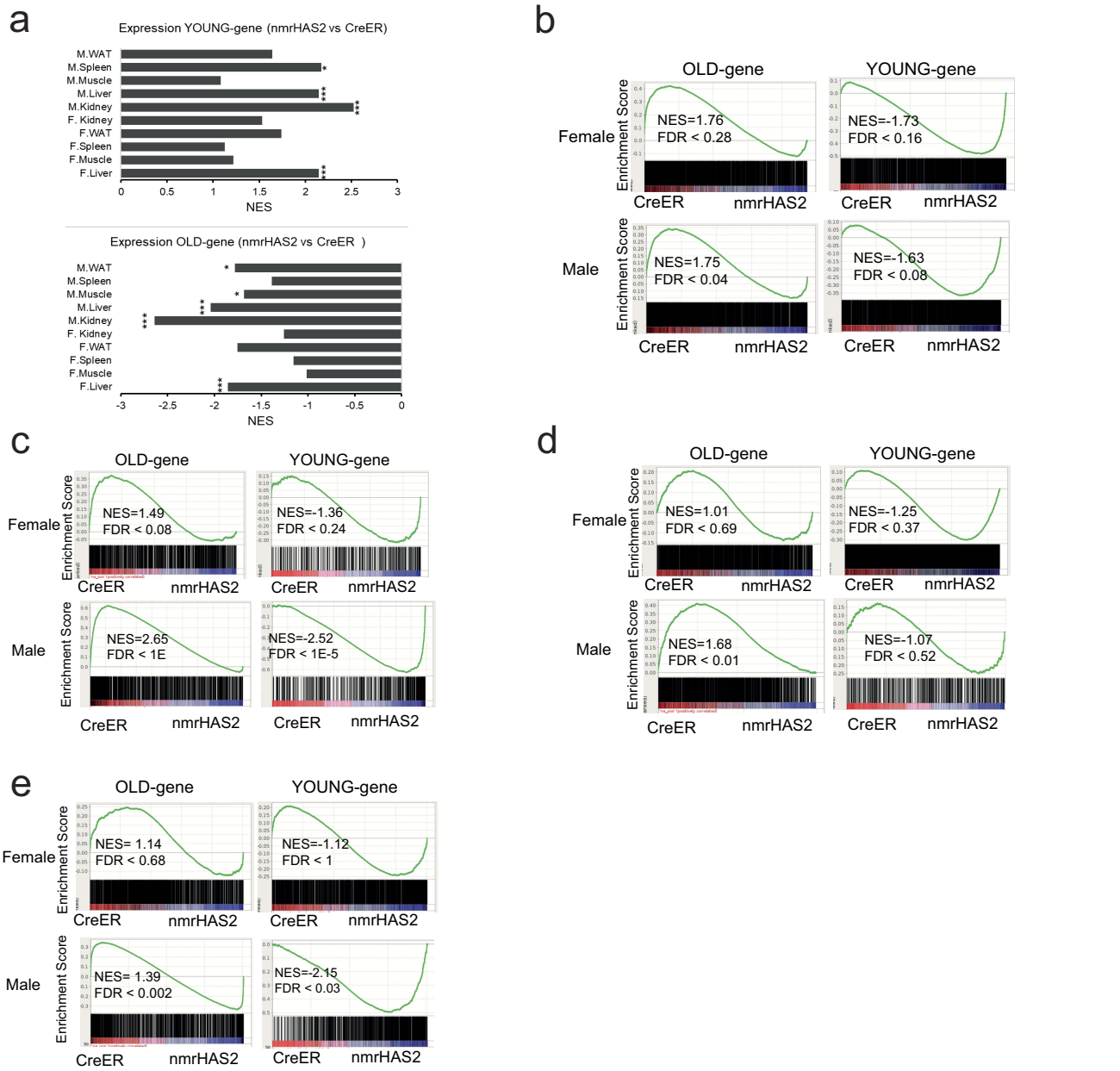

Extended Data Fig. 4 | nmrHAS2 mice showed a younger transcriptomic state. a. GSEA plots show that YOUNG gene set is upregulated, and OLD gene set is downregulated in all sequenced old nmrHAS2 mice of both sexes. * FDR<0.05, *** FDR<0.001. Exact FDR values are shown in Extended Data Fig. 4 **b**–**e**. **b**. GSEA plots showing that OLD gene set is downregulated in WAT of old male nmrHAS2 mice. **c**. GSEA plots showing that that YOUNG gene set is upregulated, and OLD gene set is downregulated in the kidney of old male nmrHAS2 mice. **d**. GSEA plots showing that OLD gene set is downregulated in the muscle of old male nmrHAS2 mice. **e**. GSEA plots showing that that YOUNG gene set is upregulated, and OLD gene set is downregulated in the spleen of old male nmrHAS2 mice.

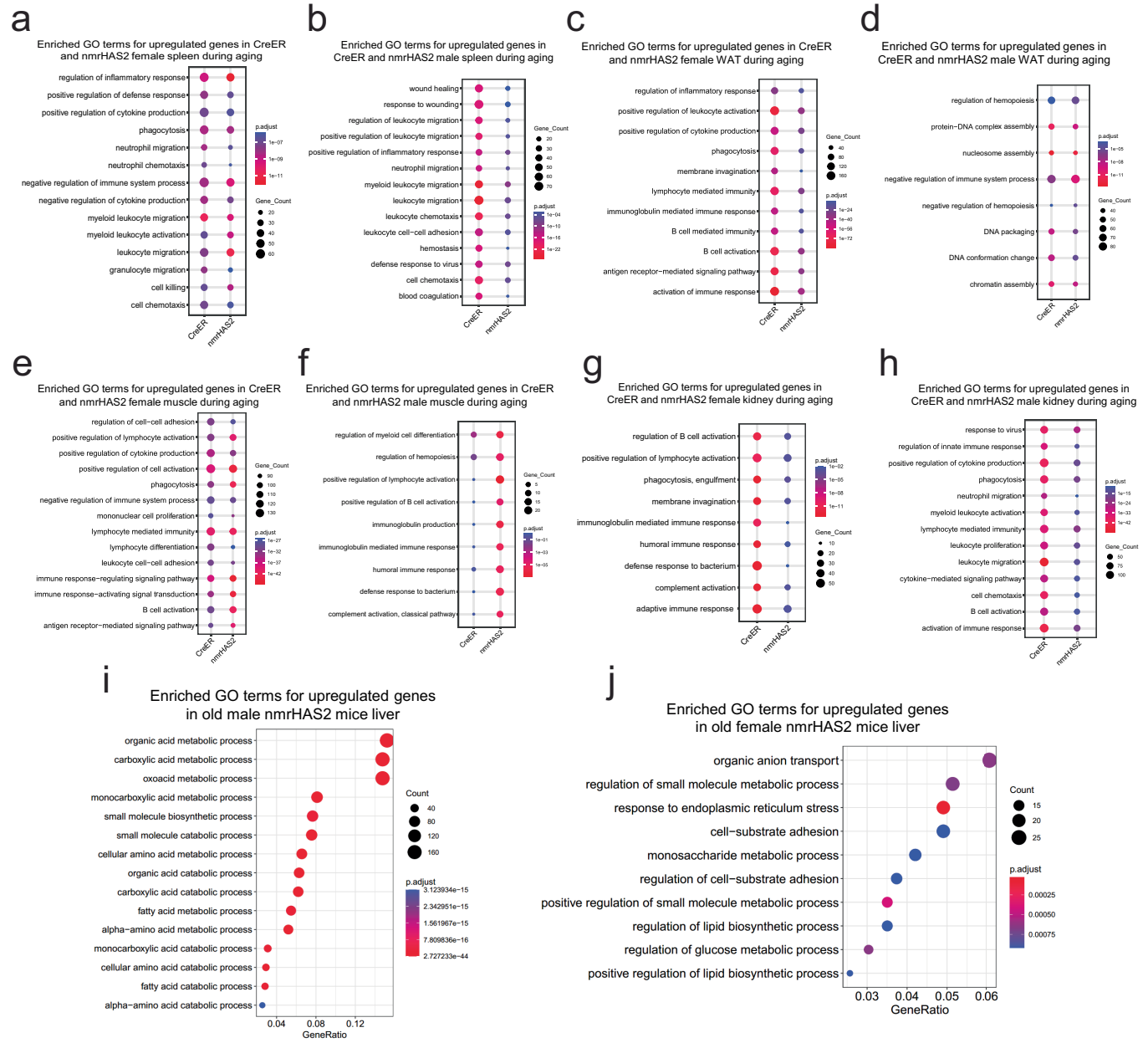

Extended Data Fig. 5 | RNAseq shows reduced inflammation during aging in nmrHAS2 mice. a-b. Enriched GO terms for upregulated genes in the spleens of CreER and nmrHAS2 female (**a**) and male mice (**b**) during aging. **c-d.** Enriched GO terms for upregulated genes in the WAT of CreER and nmrHAS2 female (**c**) and male (**d**) mice during aging. **e-f.** Enriched GO terms for upregulated genes in the muscle of CreER and nmrHAS2 female (**e**) and male (**f**) mice during aging. **g-h.** Enriched GO terms for upregulated genes in the kidneys of CreER and nmrHAS2 females (**g**) and males (**h**) during aging. **i-j.** Enriched GO terms for upregulated genes in the livers of old male (**i**) and female (**j**) nmrHAS2 mice.

	Young CreER (n=7)		Young nmrHAS2 (n=7)		Old CreER (n=7)		Old nmrHAS2 (n=7)	
Target	Mean(pg/ml)	STDEV	Mean(pg/ml)	STDEV	Mean(pg/ml)	STDEV	Mean(pg/ml)	STDEV
IL-13	2.61	1.51	2.98	3.23	31.76	80.66	2.84	3.83
IL-23	13.32	14.58	4.14	2.39	34.01	88.48	3.24	4.21
IL-12p70	4.47	0.97	4.13	1.98	6.06	5.07	4.65	1.64
TNF alpha	1.83	2.39	0.44	0.82	4.63	7.15	1.98	1.84
MCP-1 (CCL2)	Not detectable	NaN	Not detectable	NaN	48.64	66.63	Not detectable	NaN
MIP-1 beta (CCL4)	1.76	0.54	1.14	0.38	7.08	14.05	2.68	2.44
G-CSF (CSF-3)	1.89	2.08	1.42	1.8	1.7	2.15	1.28	2.44
IL-10	13.31	8.07	11.01	7.77	7.61	12.99	12.76	17.75
IL-3	0.48	0.3	0.38	0.34	0.23	0.19	0.65	1.46
LIF	Not detectable	NaN	Not detectable	NaN	Not detectable	NaN	Not detectable	NaN
IL-1 beta	0.09	0.07	Not detectable	NaN	Not detectable	NaN	Not detectable	NaN
IL-2	22.35	25.04	38.31	28.26	Not detectable	NaN	Not detectable	NaN
M-CSF	0.62	0.39	0.53	0.25	Not detectable	NaN	Not detectable	NaN
IP-10 (CXCL10)	226.4	112.34	192.9	29.33	220.88	100.96	215.13	74.67
IL-4	0.31	0.32	0.19	0.16	0.08	0.14	0.35	0.58
IL-5	5.28	1.47	9.01	4.81	5.64	4.35	2.6	1.74
IL-6	4.72	3.29	4.64	4.26	25.02	22.02	26.85	34.41
IFN alpha	Not detectable	NaN	Not detectable	NaN	Not detectable	NaN	Not detectable	NaN
IL-22	52.88	35.31	51.15	26.44	26.78	22.52	55.58	33.01
IL-9	30.28	16.65	67.2	84.01	61.81	73.1	20.57	46.19
IL-27	56.76	24.46	96.08	52.14	51.45	49.88	31.61	10.69
IFN gamma	Not detectable	NaN	Not detectable	NaN	Not detectable	NaN	Not detectable	NaN
GM-CSF	Not detectable	NaN	Not detectable	NaN	Not detectable	NaN	Not detectable	NaN
GRO alpha (CXCL1)	44.62	37.7	42.41	43.54	11.12	9.17	7.85	6.97
RANTES (CCL5)	53.49	22.07	49.43	17.43	34.87	14.67	37.58	7.84
MIP-1 alpha (CCL3)	12.9	30.92	1.44	0.79	1.66	1.37	1.11	0.75
MCP-3 (CCL7)	169.14	27.82	160.57	37.25	122.53	94.67	159.51	61.8
IL-17A (CTLA-8)	2.73	1.68	2.24	1.27	1.15	0.6	1.61	1.96
IL-15	3.22	1.07	1.75	0.45	Not detectable	NaN	Not detectable	NaN
MIP-2 alpha (CXCL2)	24.37	2.99	21.79	4.25	21.76	4.47	22.18	4.99
IL-1 alpha	2.56	1.62	2.93	1.83	Not detectable	NaN	Not detectable	NaN
ENA-78 (CXCL5)	952.05	671.65	783.3	460.49	420.13	877.39	755.14	863.53
Eotaxin (CCL11)	5480.45	1603.8	4306.84	1802.2	680.87	646.21	905.17	871.18
IL-28	18.61	17.61	8.46	10.77	9.83	12.65	23.64	25.86
IL-18	Not detectable	NaN	Not detectable	NaN	Not detectable	NaN	Not detectable	NaN
IL-31	5.69	4.77	1.85	2.03	3.49	3.3	8.27	11.62

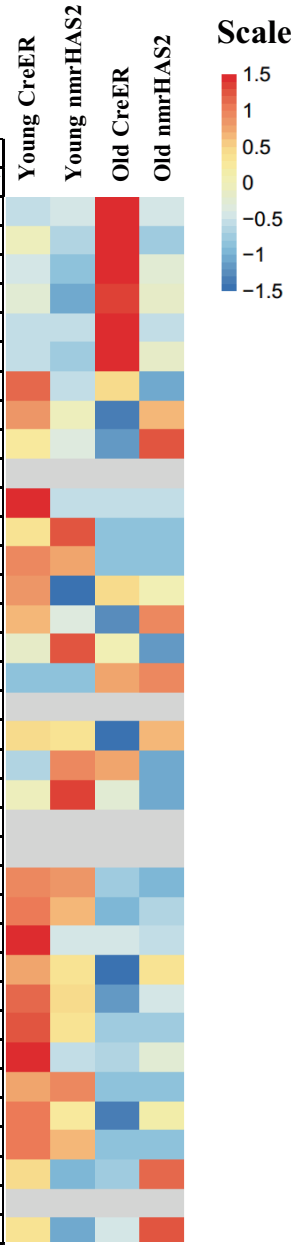

Extended Data Fig. 6 | Mean plasma concentrations of 36 inflammatory cytokines in nmrHAS2 and CreER male mice. Mean plasma concentrations of 36 inflammatory cytokines and chemokines of young (5-months) and old (24-months) male mice. The heatmap is presented alongside the value chart. In the heatmap, the levels of each target were scale automatically using R.

	Young CreER (n=11)		(n=11)		Old CreER (n=8)		Old nmrHAS2 (n=7)	
Target	Mean(pg/ml)	STDEV	Mean(pg/ml)	STDEV	Mean(pg/ml)	STDEV	Mean(pg/ml)	STDEV
IL-13	2.93	4.39	3.08	6.01	119.14	219.81	4.7	10.83
IL-23	5.42	3.41	13.19	28.97	82.22	145.06	14.13	21.4
IL-12p70	3.32	2.14	2.65	1.32	23.49	27.11	5.44	3.03
TNF alpha	0.97	2.39	1.37	2.47	26.02	26.26	6.11	4.9
MCP-1 (CCL2)	Not detectable	NaN	Not detectable	NaN	168.91	189.82	Not detectable	NaN
MIP-1 beta (CCL4)	1.18	0.89	1.06	0.5	13.1	12.78	3.08	1.59
G-CSF (CSF-3)	0.97	1.38	0.57	1.02	169.71	309.9	12.67	14.29
IL-10	5.15	3.49	3.01	3.88	449	841.23	33.48	46.48
IL-3	0.16	0.08	0.12	0.05	58.18	107.54	2.98	4.14
LIF	Not detectable	NaN	Not detectable	NaN	Not detectable	NaN	Not detectable	NaN
IL-1 beta	0.1	0.18	0.19	0.57	1.99	4.06	0.62	1.12
IL-2	25.96	36.8	36.68	43.87	66.69	130.96	5.98	12.95
M-CSF	0.41	0.25	0.2	0.2	20.17	36.99	0.98	1.89
IP-10 (CXCL10)	196.93	29.5	189.24	69.44	469.66	243.46	209.97	57.86
IL-4	0.16	0.12	0.21	0.2	48.71	97.11	1.4	3.57
IL-5	10.3	4.53	9.68	4.77	70.12	96.78	13.43	9.34
IL-6	1.55	1.24	2.89	7.1	398.54	712.97	65.92	75.46
IFN alpha	Not detectable	NaN	Not detectable	NaN	Not detectable	NaN	Not detectable	NaN
IL-22	38.5	12.63	29.53	13.46	4129	8240.58	148.6	107.75
IL-9	47.51	84.16	58.33	90.98	13599.91	30726.4	62.14	151.57
IL-27	60.21	34.08	61.74	51.79	145.87	213.1	39.69	23.4
IFN gamma	Not detectable	NaN	Not detectable	NaN	Not detectable	NaN	Not detectable	NaN
GM-CSF	Not detectable	NaN	Not detectable	NaN	85.14	166.51	7.77	11.05
GRO alpha (CXCL1)	26.18	12.54	15.79	16.68	157.51	303.44	20.57	16.23
RANTES (CCL5)	58.9	19.53	52.04	18.58	205.2	255.34	42.05	9.03
MIP-1 alpha (CCL3)	1.69	1.75	1.21	0.72	6.27	8.99	1.16	0.64
MCP-3 (CCL7)	189.85	47.22	167.74	41.96	325.29	137.79	213.83	96.4
IL-17A (CTLA-8)	2.53	2.5	1.78	1.09	271.39	516.37	10.69	8.64
IL-15	0.92	0.97	0.56	0.82	210.97	389.01	22.77	34.47
MIP-2 alpha (CXCL2)	21.93	2.34	19.93	2.45	103.54	144.43	28.36	17.15
IL-1 alpha	1.44	1.49	2.58	3.09	Not detectable	NaN	Not detectable	NaN
ENA-78 (CXCL5)	940.74	517.95	1389.74	1910.5	1750.79	3123.48	405.31	472.11
Eotaxin (CCL11)	4385.86	1312	3574.61	1563.6	697.64	427.71	767.34	419.22
IL-28	16.25	4.19	16.6	16.64	2761.36	5219.16	146.74	234.32
IL-18	Not detectable	NaN	Not detectable	NaN	2306.51	4575.61	211.87	361.93
IL-31	Not detectable	NaN	Not detectable	NaN	395.99	731.67	63.92	104.35

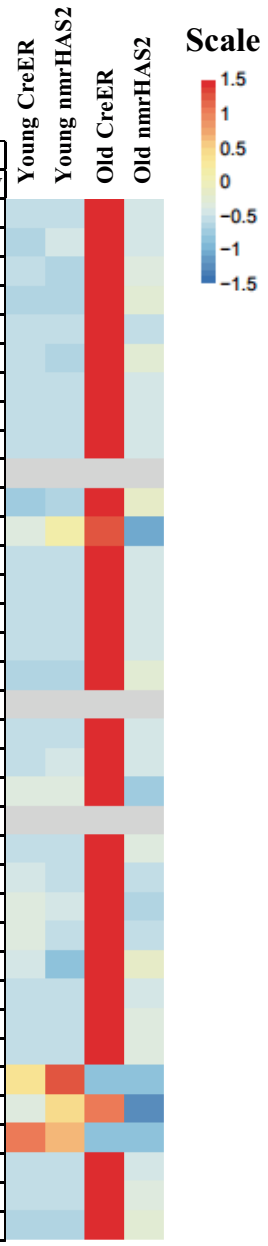

Extended Data Fig. 7 | Mean plasma concentrations of 36 inflammatory cytokines in nmrHAS2 and CreER female mice. The mean plasma concentrations of 36 inflammatory cytokines and chemokines in young (5-months) and old (24-months) female mice. The heatmap is presented alongside the value chart. In the heatmap, the levels of each target were scaled automatically using R.

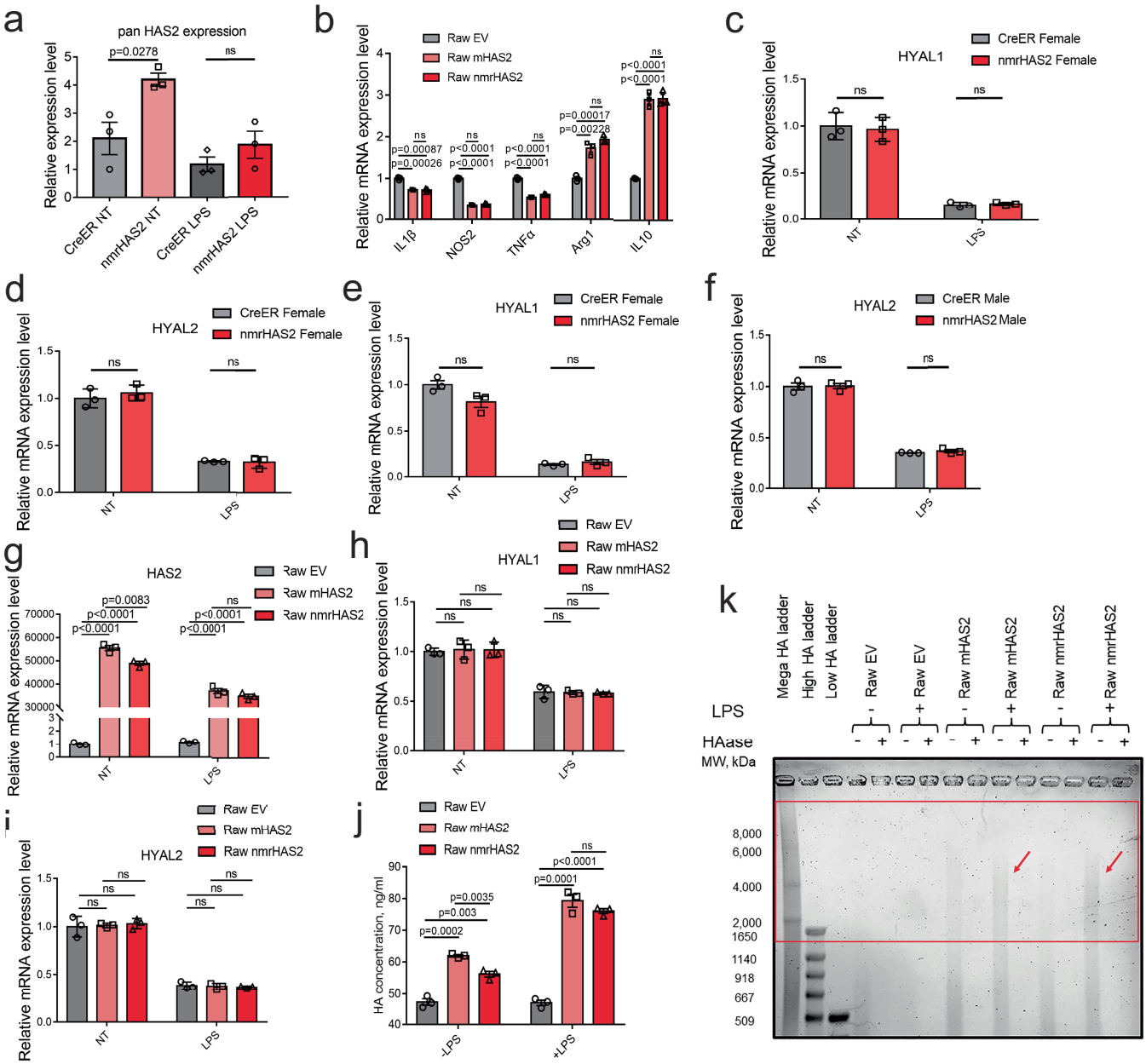

Extended Data Fig. 8 | nmrHAS2 reduces pro-inflammatory response *in vitro*. **a**. BMDM from nmrHAS2 mice have significantly upregulated HAS2 levels. BMDM were isolated from 5-months old female mice (n = 3). **b**. Raw264.7 cells overexpressing mHAS2 or nmrHAS2 show lower levels of pro-inflammatory cytokines and higher levels of anti-inflammatory cytokines. Data was normalized to Raw EV. n = 3. **c**. HYAL1 levels decrease after LPS treatment in BMDM from female mice. Normalization to CreER NT. n = 3. **d**. HYAL2 levels decrease after LPS treatment in BMDM from female mice. Normalization to CreER NT. n = 3. **e**. HYAL1 levels decrease after LPS treatment in BMDM from male mice. Normalization to CreER NT. n = 3. **f**. HYAL2 levels decrease after LPS treatment in BMDM from male mice. Normalization to CreER NT. n = 3. **g**. HAS2 levels decrease in LPS treated HAS2 expressing Raw264.7 cells. Normalization to Raw EV NT. n = 3. **h**. HYAL1 levels decrease after LPS treatment in HAS2 expressing Raw264.7 cells. Normalization to Raw EV NT. n = 3. **i**. HYAL2 levels decrease after LPS treatment in HAS2 expressing Raw264.7 cells. Normalization to Raw EV NT. n = 3. **j**. Raw264.7 cells overexpressing HAS2 produce more HA. HA ELISA was used to quantify the HA level in the media. n = 3. **k**. Raw264.7 cells overexpressing HAS2 produce more HMW-HA in the media after LPS treatment. Red square indicates the HMW-HA. Experiments were repeated for three times and showed a similar result. **a-j**. p values were calculated by two-tailed unpaired Student's t-test (p values are indicated in the graphs). Bars represent the means, error bar displays the standard error, dots represent biological replicates. Adjustments were made for multiple comparisons.

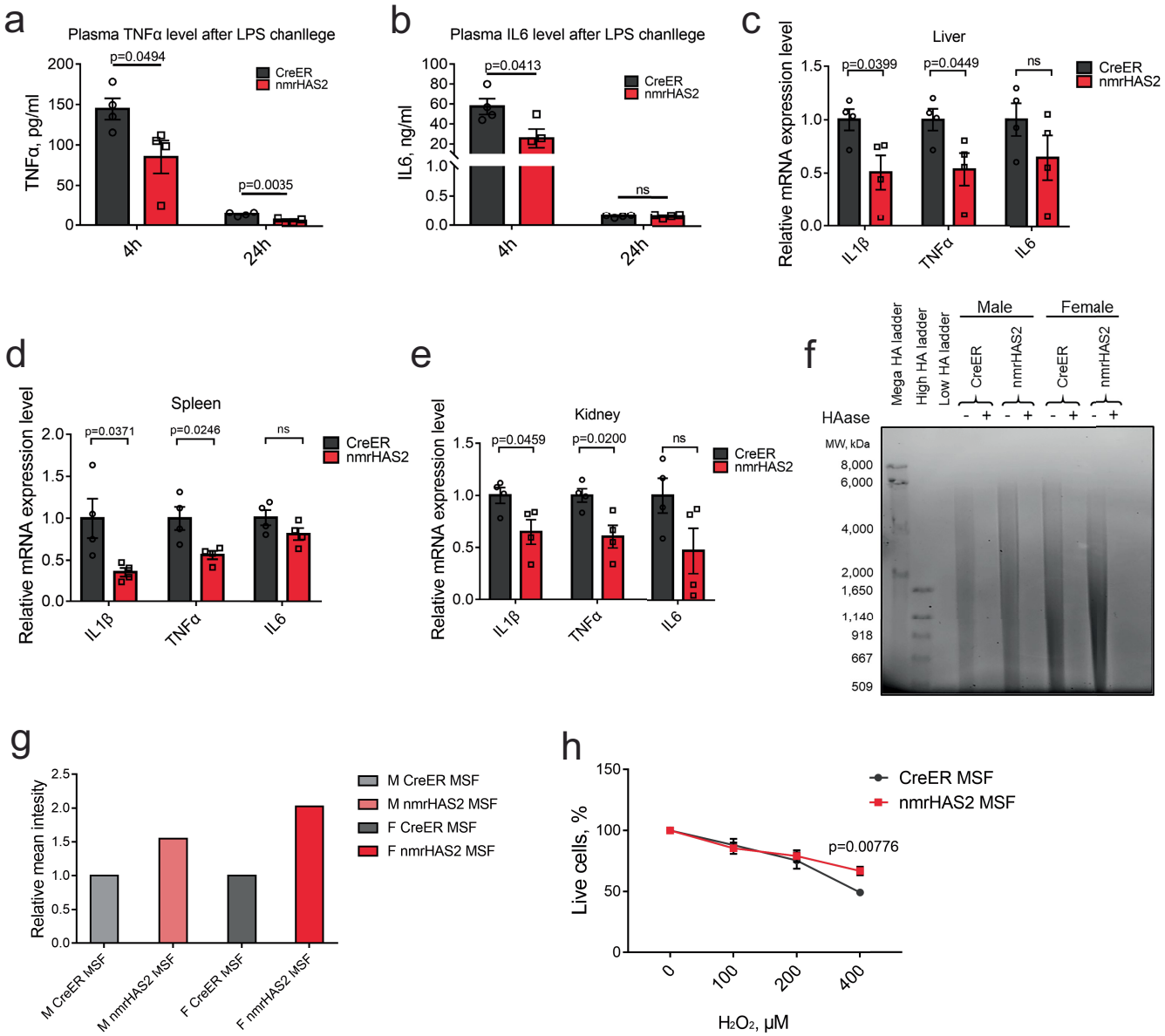

Extended Data Fig. 9 | nmrHAS2 reduces pro-inflammatory response *in vivo* and protects cells from oxidative stress. a. nmrHAS2 mice produce significantly lower plasma TNFα levels 4 h and 24 h after LPS challenge in 5-months old female mice (n = 4). **b**. nmrHAS2 mice produce significantly lower plasma IL6 levels 4 h after LPS challenge in 5- months old female mice (n = 4). **c**. nmrHAS2 mice show lower IL1β and TNFα levels in liver 24 h post LPS challenge in 5-months old female mice (n = 4). **d**. nmrHAS2 mice show lower IL1β and TNFα levels in the spleen 24 h post LPS challenge in 5- months old female mice (n = 4). **e**. nmrHAS2 mice show lower IL1β and TNFα levels in kidney 24 h post LPS challenge in 5- months old female mice (n = 4). **f**. Pulse field gel shows nmrHAS2 skin fibroblasts produce more hyaluronic acid. compared to CreER fibroblasts. HAase treated samples were run in parallel to confirm the specificity of HA staining. Media from three different cell lines was pooled for HA extraction. Experiments were repeated for three times and showed a similar result. **g**. Levels of relative on gel HA intensity. The intensity of HA was quantified using ImageJ. Intensity of nmrHAS2 group was normalized to the CreER group. **h**. Skin fibroblasts isolated from nmrHAS2 mice are more resistant to H_2O_2 treatment. Fibroblasts were isolated from 5-months old female mice (n = 4). p-values were calculated using unpaired two-tailed t-test. **a**-**e**. p values were calculated by two-tailed unpaired t-test. Bars represent the means, error bars show the standard errors, dots represent biological replicates.

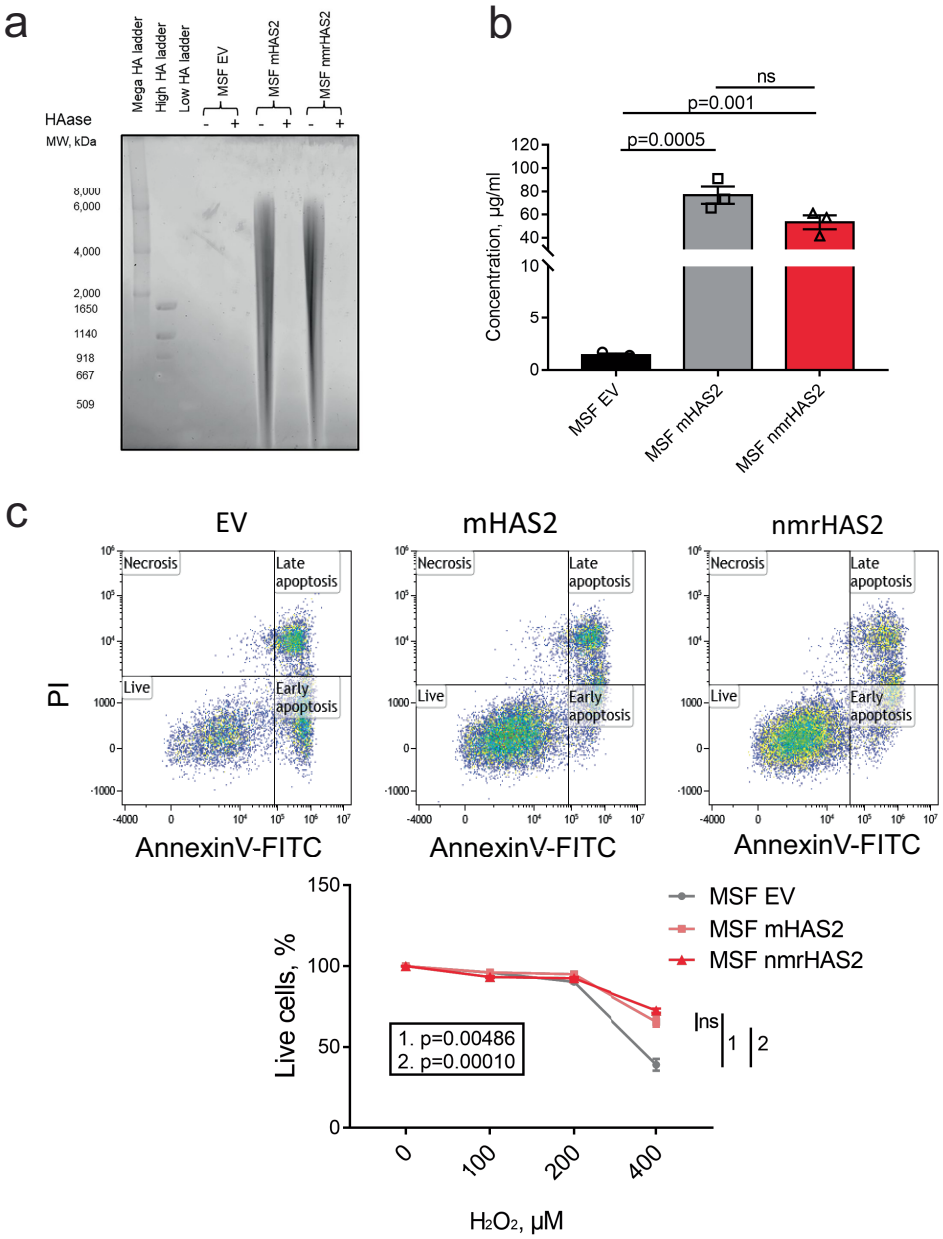

Extended Data Fig. 10 | Overexpression of mouse or nmrHAS2 protects cells from oxidative stress. a. Pulse field gel shows that mouse skin fibroblasts (MSF) overexpressing mouse HAS2 (mHAS2) or nmrHAS2 produce more hyaluronic acid compared to fibroblasts transfected with empty vector (EV). HAase-treated samples were run in parallel to confirm the specificity of HA staining. Media from three different cell lines was pooled for HA extraction. **b.** HA ELISA shows that mouse skin fibroblasts (MSF) overexpressing mHAS2 or nmrHAS2 produce more hyaluronic acid compared to fibroblasts transfected with empty vector (EV). p-values were calculated using unpaired two-tailed t-test, bars represent the means, error bars show standard errors, dots represent technical replicates. **c.** Mouse skin fibroblasts overexpressing mHAS2 or nmrHAS2 are more resistant to H_2O_2 treatment. p-values were calculated using unpaired two-tailed t-test, error bars show standard errors, dots represent technical replicates.

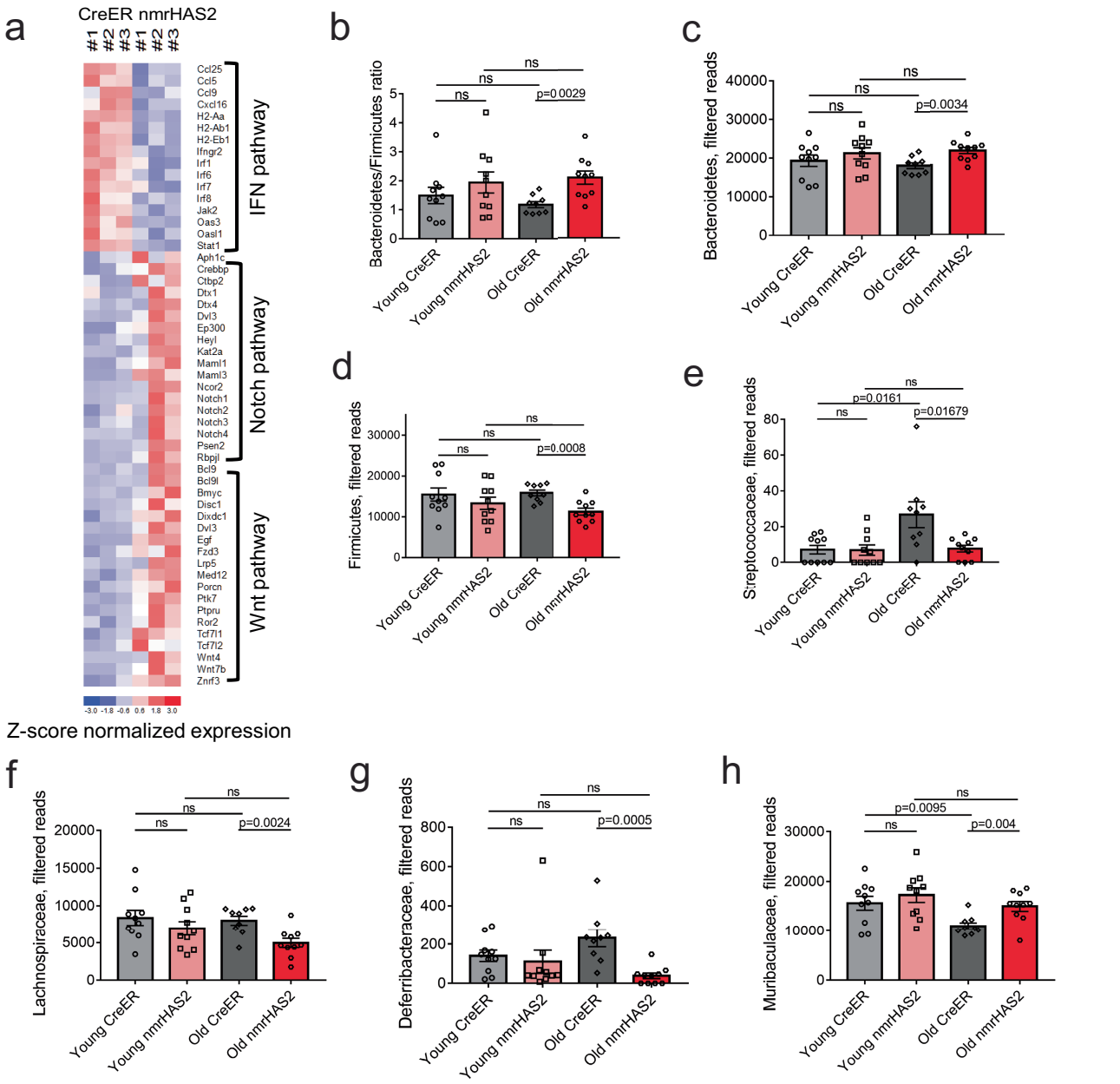

Extended Data Fig. 11 | Old nmrHAS2 mice differ from age matched CreER controls in their gut microbiome composition. a. Heatmap of genes involve in IFN, WNT, and Notch pathways. **b**. 16s rRNA sequencing shows old nmrHAS2 mice (n = 9) have a higher B/F ratio compared to age-matched controls (n = 10). Pooled females and males. **c, d**. 16s rRNA sequencing shows that at the phylum level old nmrHAS2 mice (n = 9) have more abundant *Bacteroidetes (**c**)* and less abundant *Firmicutes (**d**)* compared to age-matched controls (n = 10). 7- and 24-month-old mice were used. Pooled females and males. **e-g**. 16s rRNA sequencing shows that at family level, old nmrHAS2 mice (n = 9) have less abundant pro-inflammatory *Streptococcaceae (**e**)*, *Lachnospiraceae (**f**)*, and *Deferribacteraceae (**g**)* compared to age-matched controls (n = 10). 7- and 24-month-old mice were used. Pooled females and males. **h**. 16s rRNA sequencing shows that at family level, old nmrHAS2 mice (n = 9) have more *Muribaculaceae* compared to the age-matched controls (n = 10). Pooled females and males. **b-h**. p-values were calculated by two-tailed unpaired t-test (p-values are indicated in the graphs). Bars represent the means, error bars show standard errors, dots represent biological replicates. Adjustments were made for multiple comparisons.

Extended Data Table 1 | nmrHAS2 mRNA level in different organs

Tissue	Gender	Log2(nmrHAS2/CreER)	p value
Liver	Female	7.7	2E-09
Muscle	Female	9.5	2E-136
Spleen	Female	3.9	3E-38
WAT	Female	1.8	3E-04
Kidney	Female	10.6	1.77E-15
Intestine	Female	5.7	9E-54
Liver	Male	Not detectable	N/A
Muscle	Male	8.7	1E-17
Spleen	Male	3.0	4E-05
WAT	Male	3.2	3E-08
Kidney	Male	10.4	8.02E-08
Intestine	Male	5.1	2E-22

Extended Data Table 2 | Correlation functions signatures Spearman P_{adj} values

	Interventions: Median lifespan	Interventions: Max lifespan	Interventions: CR	Interventions: GH deficiency	Interventions: Rapamycin	Aging: Brain	Aging: Liver	Aging: Human	Aging: Rat	Aging: Mouse	Aging: Kidney	nmrHAS2: Female	nmrHAS2: Male
Interventions: Median lifespan	0	0	9.13E-204	1.85E-199	0.036998849	0.002766318	1.28E-41	2.85E-22	8.19E-34	7.94E-28	3.62E-31	1.33E-25	1.36E-81
Interventions: Max lifespan	0	0	7.08E-222	4.12E-79	1.26E-57	1.15E-52	1.68E-178	2.04E-46	1.63E-92	7.58E-160	1.03E-122	3.74E-85	9.57E-113
Interventions: CR	2.13E-204	1.36E-222	0	5.75E-42	9.34E-18	1.41E-10	5.89E-26	9.50E-08	9.74E-97	4.34E-12	6.67E-45	3.86E-92	2.87E-76
Interventions: GH deficiency	4.47E-200	2.09E-79	3.64E-42	0	6.09E-14	3.62E-14	0.038716956	0.951228974	0.678058754	0.412573705	0.073540791	1.40E-26	0.32824947
Interventions: Rapamycin	0.033298964	7.33E-58	6.93E-18	4.67E-14	0	5.32E-75	4.02E-107	4.98E-13	4.40E-62	1.71E-109	6.39E-84	3.34E-112	6.98E-23
Aging: Brain	0.00235137	6.90E-53	1.13E-10	2.74E-14	2.80E-75	0	1.03E-212	8.94E-256	1.42E-197	3.08E-271	2.39E-227	3.19E-86	1.80E-22
Aging: Liver	8.21E-42	4.47E-179	4.08E-26	0.035167902	1.58E-107	2.23E-213	0	3.83E-66	0	0	0	5.65E-259	4.89E-189
Aging: Human	2.07E-22	1.24E-46	8.00E-08	0.945146662	3.86E-13	1.49E-256	2.11E-66	0	2.47E-21	1.60E-68	7.24E-66	6.54E-41	6.31E-68
Aging: Rat	5.39E-34	7.19E-93	4.06E-97	0.661107285	2.53E-62	3.55E-198	0	1.81E-21	0	2.71E-274	0	2.13E-209	2.42E-123
Aging: Mouse	5.36E-28	2.15E-160	3.40E-12	0.395383134	6.41E-110	4.36E-272	0	8.55E-69	3.62E-275	0	0	9.21E-216	1.08E-145
Aging: Kidney	2.41E-31	3.44E-123	4.11E-45	0.067412392	3.14E-84	4.18E-228	0	4.04E-66	0	0	0	1.97E-310	2.85E-224
nmrHAS2: Female	9.33E-26	1.78E-85	1.74E-92	9.55E-27	1.22E-112	1.46E-86	8.95E-260	4.25E-41	4.79E-210	1.92E-216	1.967E-311	0	0
nmrHAS2: Male	6.81E-82	3.43E-113	1.48E-76	0.311836996	4.94E-23	1.29E-22	1.26E-189	3.42E-68	7.86E-124	3.34E-146	5.23E-225	0	0

nature portfolio

Corresponding author(s): Vera Gorbunova, Andrei Seluanov

Last updated by author(s): Jun 30, 2023

Reporting Summary

Nature Portfolio wishes to improve the reproducibility of the work that we publish. This form provides structure for consistency and transparency in reporting. For further information on Nature Portfolio policies, see our Editorial Policies and the Editorial Policy Checklist.

Statistics

For all statistical analyses, confirm that the following items are present in the figure legend, table legend, main text, or Methods section.

n/a	Confirmed
☐	☒ The exact sample size (*n*) for each experimental group/condition, given as a discrete number and unit of measurement
☐	☒ A statement on whether measurements were taken from distinct samples or whether the same sample was measured repeatedly
☐	☒ The statistical test(s) used AND whether they are one- or two-sided *Only common tests should be described solely by name; describe more complex techniques in the Methods section.*
☒	☐ A description of all covariates tested
☐	☒ A description of any assumptions or corrections, such as tests of normality and adjustment for multiple comparisons
☐	☒ A full description of the statistical parameters including central tendency (e.g. means) or other basic estimates (e.g. regression coefficient) AND variation (e.g. standard deviation) or associated estimates of uncertainty (e.g. confidence intervals)
☐	☒ For null hypothesis testing, the test statistic (e.g. *F*, *t*, *r*) with confidence intervals, effect sizes, degrees of freedom and *P* value noted *Give P values as exact values whenever suitable.*
☒	☐ For Bayesian analysis, information on the choice of priors and Markov chain Monte Carlo settings
☐	☒ For hierarchical and complex designs, identification of the appropriate level for tests and full reporting of outcomes
☐	☒ Estimates of effect sizes (e.g. Cohen's *d*, Pearson's *r*), indicating how they were calculated

Our web collection on statistics for biologists contains articles on many of the points above.

Software and code

Policy information about availability of computer code

Data collection	The publicly available RNAseq data was downloaded from GEO using SRA toolkit provided by NCBI.
Data analysis	The RNA-seq reads were first processed using Trim_Galore (version 0.6.6), which trimmed both adapter sequences and low-quality base calls (Phred quality score < 20). The clean RNA-seq reads were used to quantify the gene expression with Salmon (version 1.4.0). Specific parameters (--useVBOpt --seqBias --gcBias) were set for sequence-specific bias correction and fragment GC bias correction. Gencode (version M25) was used for the genome-wide annotation of the gene in the mouse. The reads counts for genes were used as the input for differential expression analysis by DESeq2. Gene set enrichment analysis (GSEA) was performed with "Preranked" model (version 4.1.0). GO analysis were performed by R package clusterProfiler (Release version 3.14). The Illumina Miseq microbiome data analysis was carried out with a workflow employing the Quantitative Insights Into Microbial Ecology (QIIME2) pipeline. Pairwise Spearman correlation between logFC induced by nmrHas2 expression and associated with signatures of aging, lifespan-extending interventions, and longevity was calculated based on the union of top 400 statistically significant genes (with the lowest p-value) for each pair of signatures. For the identification of enriched functions affected by nmrHas2 expression in mouse livers we performed Fisher exact test and functional GSEA on a pre-ranked list of genes based on log10(p-value) corrected by the sign of regulation, calculated as: -(pv)*sgn(lfc), where pv and lfc are p-value and logFC of a certain gene, respectively, obtained from edgeR output, and sgn is the signum function (equal to 1, -1 and 0 if value is positive, negative or equal to 0, respectively). HALLMARK, KEGG and REACTOME ontologies from the Molecular Signature Database (MSigDB) were used as gene sets. Fisher exact test and GSEA were performed separately for each sex using gprofile2 and fgsea R packages, respectively. A q-value cutoff of 0.1 was used to select statistically significant functions. Data are shown as means with SEM (unless stated otherwise). N indicates the number of animals per test group; age and sex are also noted. The number of animals chose for each experiment was calculated using power analysis. Randomly picked littermates were used for all the

experiments. Student's t test (unpaired, two-tailed, equal variance) was used for all pairwise comparisons which satisfied with normal distribution. Mann-Whitney u test was used for data which is not satisfied with normal distribution. All relevant p values are shown in the figures; p<0.0001 was displayed as 'p<0.0001', and ns means no significance. Demographic data were processed with GraphPad Prism software to compute mean and median lifespans, SEM, percent increase of the median, and p values (log-rank test) for each cohort.

For manuscripts utilizing custom algorithms or software that are central to the research but not yet described in published literature, software must be made available to editors and reviewers. We strongly encourage code deposition in a community repository (e.g. GitHub). See the Nature Portfolio guidelines for submitting code & software for further information.

Data

Policy information about availability of data

All manuscripts must include a data availability statement. This statement should provide the following information, where applicable:

- Accession codes, unique identifiers, or web links for publicly available datasets
- A description of any restrictions on data availability
- For clinical datasets or third party data, please ensure that the statement adheres to our policy

The RNA-Seq data, epigenetic clock data, and 16S rDNA sequencing data produced in this paper have been deposited in the Gene Expression Omnibus (GSE234563, GSE234154, GSE234286).

Human research participants

Policy information about studies involving human research participants and Sex and Gender in Research.

Reporting on sex and gender	No human samples or data has been used in this study.
Population characteristics	No human samples or data has been used in this study.
Recruitment	No human samples or data has been used in this study.
Ethics oversight	No human samples or data has been used in this study.

Note that full information on the approval of the study protocol must also be provided in the manuscript.

Field-specific reporting

Please select the one below that is the best fit for your research. If you are not sure, read the appropriate sections before making your selection.

☒ Life sciences ☐ Behavioural & social sciences ☐ Ecological, evolutionary & environmental sciences

For a reference copy of the document with all sections, see nature.com/documents/nr-reporting-summary-flat.pdf

Life sciences study design

All studies must disclose on these points even when the disclosure is negative.

Sample size	Power analysis was used to determine the samples size of each study.
Data exclusions	No data was excluded from the analysis
Replication	All the experiments in this study have enough biological replicates and were technically repeated for at least three time.
Randomization	All the transgenic mice used in this study were randomly picked. Their litter mates were used as controls.
Blinding	All investigators were blinded when collecting data.

Behavioural & social sciences study design

All studies must disclose on these points even when the disclosure is negative.

Study description	*Briefly describe the study type including whether data are quantitative, qualitative, or mixed-methods (e.g. qualitative cross-sectional, quantitative experimental, mixed-methods case study).*
Research sample	*State the research sample (e.g. Harvard university undergraduates, villagers in rural India) and provide relevant demographic*

Research sample	*information (e.g. age, sex) and indicate whether the sample is representative. Provide a rationale for the study sample chosen. For studies involving existing datasets, please describe the dataset and source.*
Sampling strategy	*Describe the sampling procedure (e.g. random, snowball, stratified, convenience). Describe the statistical methods that were used to predetermine sample size OR if no sample-size calculation was performed, describe how sample sizes were chosen and provide a rationale for why these sample sizes are sufficient. For qualitative data, please indicate whether data saturation was considered, and what criteria were used to decide that no further sampling was needed.*
Data collection	*Provide details about the data collection procedure, including the instruments or devices used to record the data (e.g. pen and paper, computer, eye tracker, video or audio equipment) whether anyone was present besides the participant(s) and the researcher, and whether the researcher was blind to experimental condition and/or the study hypothesis during data collection.*
Timing	*Indicate the start and stop dates of data collection. If there is a gap between collection periods, state the dates for each sample cohort.*
Data exclusions	*If no data were excluded from the analyses, state so OR if data were excluded, provide the exact number of exclusions and the rationale behind them, indicating whether exclusion criteria were pre-established.*
Non-participation	*State how many participants dropped out/declined participation and the reason(s) given OR provide response rate OR state that no participants dropped out/declined participation.*
Randomization	*If participants were not allocated into experimental groups, state so OR describe how participants were allocated to groups, and if allocation was not random, describe how covariates were controlled.*

Ecological, evolutionary & environmental sciences study design

All studies must disclose on these points even when the disclosure is negative.

Study description	*Briefly describe the study. For quantitative data include treatment factors and interactions, design structure (e.g. factorial, nested, hierarchical), nature and number of experimental units and replicates.*
Research sample	*Describe the research sample (e.g. a group of tagged Passer domesticus, all Stenocereus thurberi within Organ Pipe Cactus National Monument), and provide a rationale for the sample choice. When relevant, describe the organism taxa, source, sex, age range and any manipulations. State what population the sample is meant to represent when applicable. For studies involving existing datasets, describe the data and its source.*
Sampling strategy	*Note the sampling procedure. Describe the statistical methods that were used to predetermine sample size OR if no sample-size calculation was performed, describe how sample sizes were chosen and provide a rationale for why these sample sizes are sufficient.*
Data collection	*Describe the data collection procedure, including who recorded the data and how.*
Timing and spatial scale	*Indicate the start and stop dates of data collection, noting the frequency and periodicity of sampling and providing a rationale for these choices. If there is a gap between collection periods, state the dates for each sample cohort. Specify the spatial scale from which the data are taken*
Data exclusions	*If no data were excluded from the analyses, state so OR if data were excluded, describe the exclusions and the rationale behind them, indicating whether exclusion criteria were pre-established.*
Reproducibility	*Describe the measures taken to verify the reproducibility of experimental findings. For each experiment, note whether any attempts to repeat the experiment failed OR state that all attempts to repeat the experiment were successful.*
Randomization	*Describe how samples/organisms/participants were allocated into groups. If allocation was not random, describe how covariates were controlled. If this is not relevant to your study, explain why.*
Blinding	*Describe the extent of blinding used during data acquisition and analysis. If blinding was not possible, describe why OR explain why blinding was not relevant to your study.*

Did the study involve field work? ☐ Yes ☐ No

Field work, collection and transport

Field conditions	*Describe the study conditions for field work, providing relevant parameters (e.g. temperature, rainfall).*
Location	*State the location of the sampling or experiment, providing relevant parameters (e.g. latitude and longitude, elevation, water depth).*
Access & import/export	*Describe the efforts you have made to access habitats and to collect and import/export your samples in a responsible manner and in*

Access & import/export	*compliance with local, national and international laws, noting any permits that were obtained (give the name of the issuing authority, the date of issue, and any identifying information).*
Disturbance	*Describe any disturbance caused by the study and how it was minimized.*

Reporting for specific materials, systems and methods

We require information from authors about some types of materials, experimental systems and methods used in many studies. Here, indicate whether each material, system or method listed is relevant to your study. If you are not sure if a list item applies to your research, read the appropriate section before selecting a response.

Materials & experimental systems

n/a	Involved in the study
☐	☒ Antibodies
☐	☒ Eukaryotic cell lines
☒	☐ Palaeontology and archaeology
☐	☒ Animals and other organisms
☒	☐ Clinical data
☒	☐ Dual use research of concern

Methods

n/a	Involved in the study
☒	☐ ChIP-seq
☐	☒ Flow cytometry
☒	☐ MRI-based neuroimaging

Antibodies

Antibodies used	Rabbit polyclonal anti-MUC2 (GeneTex, Cat#GTX100664), Rabbit monoclonal anti- Lyzozyme (Abcam, Cat#ab108508), Goat anti Rabbit IgG (H+L) Secondary Antibody, Alexa Fluor 568 (Invitrogen, Cat#A11011)
Validation	The validation of primary antibodies used in this study could be found use the following links. https://www.genetex.com/Product/Detail/MUC2-antibody-C3-C-term/GTX100664#references https://www.abcam.com/lysozyme-antibody-epr29942-ab108508.html

Eukaryotic cell lines

Policy information about cell lines and Sex and Gender in Research

Cell line source(s)	Primary mouse skin fibroblast and bone marrow derived macrophages were isolated from control and nmrHAS2 mice. Raw264.7 cell line was obtained from ATCC. Mouse skin fibroblast and Raw264.7 cells overexpressing mHAS2 or nmrHAS2 were generated in this study.
Authentication	None of the cell lines used were authenticated.
Mycoplasma contamination	Cell lines were all tested negative for mycoplasma contamination.
Commonly misidentified lines (See ICLAC register)	N/A

Palaeontology and Archaeology

Specimen provenance	*Provide provenance information for specimens and describe permits that were obtained for the work (including the name of the issuing authority, the date of issue, and any identifying information). Permits should encompass collection and, where applicable, export.*
Specimen deposition	*Indicate where the specimens have been deposited to permit free access by other researchers.*
Dating methods	*If new dates are provided, describe how they were obtained (e.g. collection, storage, sample pretreatment and measurement), where they were obtained (i.e. lab name), the calibration program and the protocol for quality assurance OR state that no new dates are provided.*

☐ Tick this box to confirm that the raw and calibrated dates are available in the paper or in Supplementary Information.

Ethics oversight	*Identify the organization(s) that approved or provided guidance on the study protocol, OR state that no ethical approval or guidance was required and explain why not.*

Note that full information on the approval of the study protocol must also be provided in the manuscript.

Animals and other research organisms

Policy information about studies involving animals; ARRIVE guidelines recommended for reporting animal research, and Sex and Gender in Research

Laboratory animals	All the mice used in this study are on C57Bl6 background. The nmrHAS2 transgenic mouse strain is generated in this study. B6.129-Gt(ROSA)26Sortm1(cre/ERT2)Tyj/J mice were from Jackson lab. The information of this strain could be found using the following link. https://www.jax.org/strain/008463
Wild animals	This study did not use any wild animal samples.
Reporting on sex	Both female and male mouse samples were used in this study without bias.
Field-collected samples	No field-collected samples were used in this study.
Ethics oversight	All animal experiments in this study were approved and performed in accordance with guidelines set forth by the University of Rochester Committee on Animal Resources with protocol number 2017-033 (mouse).

Note that full information on the approval of the study protocol must also be provided in the manuscript.

Clinical data

Policy information about clinical studies

All manuscripts should comply with the ICMJE guidelines for publication of clinical research and a completed CONSORT checklist must be included with all submissions.

Clinical trial registration	*Provide the trial registration number from ClinicalTrials.gov or an equivalent agency.*
Study protocol	*Note where the full trial protocol can be accessed OR if not available, explain why.*
Data collection	*Describe the settings and locales of data collection, noting the time periods of recruitment and data collection.*
Outcomes	*Describe how you pre-defined primary and secondary outcome measures and how you assessed these measures.*

Dual use research of concern

Policy information about dual use research of concern

Hazards

Could the accidental, deliberate or reckless misuse of agents or technologies generated in the work, or the application of information presented in the manuscript, pose a threat to:

No	Yes	
☐	☐	Public health
☐	☐	National security
☐	☐	Crops and/or livestock
☐	☐	Ecosystems
☐	☐	Any other significant area

Experiments of concern

Does the work involve any of these experiments of concern:

No	Yes	
☐	☐	Demonstrate how to render a vaccine ineffective
☐	☐	Confer resistance to therapeutically useful antibiotics or antiviral agents
☐	☐	Enhance the virulence of a pathogen or render a nonpathogen virulent
☐	☐	Increase transmissibility of a pathogen
☐	☐	Alter the host range of a pathogen
☐	☐	Enable evasion of diagnostic/detection modalities
☐	☐	Enable the weaponization of a biological agent or toxin
☐	☐	Any other potentially harmful combination of experiments and agents

ChIP-seq

Data deposition

☐ Confirm that both raw and final processed data have been deposited in a public database such as GEO.

☐ Confirm that you have deposited or provided access to graph files (e.g. BED files) for the called peaks.

Data access links *May remain private before publication.*	*For "Initial submission" or "Revised version" documents, provide reviewer access links. For your "Final submission" document, provide a link to the deposited data.*
Files in database submission	*Provide a list of all files available in the database submission.*
Genome browser session (e.g. UCSC)	*Provide a link to an anonymized genome browser session for "Initial submission" and "Revised version" documents only, to enable peer review. Write "no longer applicable" for "Final submission" documents.*

Methodology

Replicates	*Describe the experimental replicates, specifying number, type and replicate agreement.*
Sequencing depth	*Describe the sequencing depth for each experiment, providing the total number of reads, uniquely mapped reads, length of reads and whether they were paired- or single-end.*
Antibodies	*Describe the antibodies used for the ChIP-seq experiments; as applicable, provide supplier name, catalog number, clone name, and lot number.*
Peak calling parameters	*Specify the command line program and parameters used for read mapping and peak calling, including the ChIP, control and index files used.*
Data quality	*Describe the methods used to ensure data quality in full detail, including how many peaks are at FDR 5% and above 5-fold enrichment.*
Software	*Describe the software used to collect and analyze the ChIP-seq data. For custom code that has been deposited into a community repository, provide accession details.*

Flow Cytometry

Plots

Confirm that:

☒ The axis labels state the marker and fluorochrome used (e.g. CD4-FITC).

☒ The axis scales are clearly visible. Include numbers along axes only for bottom left plot of group (a 'group' is an analysis of identical markers).

☒ All plots are contour plots with outliers or pseudocolor plots.

☒ A numerical value for number of cells or percentage (with statistics) is provided.

Methodology

Sample preparation	Skin fibroblast cells under population doubling 15 were used for H2O2 treatment. Cells with ~80% confluency were treated with H2O2 at concentrations of 100 µM, 200 µM, and 400 µM for 24h. Cells were collected, and apoptotic cells were quantified using Annexin V FLUOS Staining Kit (Roche) following the manufacturer's instructions.
Instrument	CytoFlexS flow cytometer (Beckman)
Software	Kaluza (Beckman) was used to analyze flow data.
Cell population abundance	One million gated cells were used for the analysis.
Gating strategy	The gating strategy is shown in figure 5j. Cells which are double negative for Annexin-V and PI signals were defined as live cells.

☒ Tick this box to confirm that a figure exemplifying the gating strategy is provided in the Supplementary Information.

Magnetic resonance imaging

Experimental design

Design type	*Indicate task or resting state; event-related or block design.*

Design specifications

Specify the number of blocks, trials or experimental units per session and/or subject, and specify the length of each trial or block (if trials are blocked) and interval between trials.

Behavioral performance measures

State number and/or type of variables recorded (e.g. correct button press, response time) and what statistics were used to establish that the subjects were performing the task as expected (e.g. mean, range, and/or standard deviation across subjects).

Acquisition

Imaging type(s)

Specify: functional, structural, diffusion, perfusion.

Field strength

Specify in Tesla

Sequence & imaging parameters

Specify the pulse sequence type (gradient echo, spin echo, etc.), imaging type (EPI, spiral, etc.), field of view, matrix size, slice thickness, orientation and TE/TR/flip angle.

Area of acquisition

State whether a whole brain scan was used OR define the area of acquisition, describing how the region was determined.

Diffusion MRI ☐ Used ☐ Not used

Preprocessing

Preprocessing software

Provide detail on software version and revision number and on specific parameters (model/functions, brain extraction, segmentation, smoothing kernel size, etc.).

Normalization

If data were normalized/standardized, describe the approach(es): specify linear or non-linear and define image types used for transformation OR indicate that data were not normalized and explain rationale for lack of normalization.

Normalization template

Describe the template used for normalization/transformation, specifying subject space or group standardized space (e.g. original Talairach, MNI305, ICBM152) OR indicate that the data were not normalized.

Noise and artifact removal

Describe your procedure(s) for artifact and structured noise removal, specifying motion parameters, tissue signals and physiological signals (heart rate, respiration).

Volume censoring

Define your software and/or method and criteria for volume censoring, and state the extent of such censoring.

Statistical modeling & inference

Model type and settings

Specify type (mass univariate, multivariate, RSA, predictive, etc.) and describe essential details of the model at the first and second levels (e.g. fixed, random or mixed effects; drift or auto-correlation).

Effect(s) tested

Define precise effect in terms of the task or stimulus conditions instead of psychological concepts and indicate whether ANOVA or factorial designs were used.

Specify type of analysis: ☐ Whole brain ☐ ROI-based ☐ Both

Statistic type for inference
(See Eklund et al. 2016)

Specify voxel-wise or cluster-wise and report all relevant parameters for cluster-wise methods.

Correction

Describe the type of correction and how it is obtained for multiple comparisons (e.g. FWE, FDR, permutation or Monte Carlo).

Models & analysis

n/a	Involved in the study
☐	☐ Functional and/or effective connectivity
☐	☐ Graph analysis
☐	☐ Multivariate modeling or predictive analysis

Functional and/or effective connectivity

Report the measures of dependence used and the model details (e.g. Pearson correlation, partial correlation, mutual information).

Graph analysis

Report the dependent variable and connectivity measure, specifying weighted graph or binarized graph, subject- or group-level, and the global and/or node summaries used (e.g. clustering coefficient, efficiency, etc.).

Multivariate modeling and predictive analysis

Specify independent variables, features extraction and dimension reduction, model, training and evaluation metrics.